Neurobiology of Disease

Complex Synaptic and Intrinsic Interactions Disrupt Input/Output Functions in the Hippocampus of *Scn1b* Knock-Out Mice

Jessica Hotard Chancey, Alisha A. Ahmed, Fernando Isaac Guillén, Vighnesh Ghatpande, and MacKenzie A. Howard

Departments of Neurology and Neuroscience, Center for Learning and Memory, Dell Medical School, University of Texas at Austin, Austin, Texas 78712

Pathogenic variants in *SCN1B* have been linked to severe developmental epileptic encephalopathies including Dravet syndrome. *Scn1b* knock-out (KO) mice model *SCN1B* loss-of-function (LOF) disorders, demonstrating seizures, developmental delays, and early death. *SCN1B* encodes the protein β1, an ion channel auxiliary subunit that also has roles in cell adhesion, neurite outgrowth, and gene expression. The goal of this project is to better understand of how loss of *Scn1b* alters information processing in the brain, resulting in seizures and associated cognitive dysfunction. Using slice electrophysiology in the CA1 region of the hippocampus from male and female *Scn1b* KO mice and wild-type (WT) littermates, we found that processing of physiologically relevant patterned Schaffer collateral (SC) stimulation produces larger, prolonged depolarizations and increased spiking in KO neurons compared with WTs. KO neurons exhibit enhanced intrinsic excitability, firing more action potentials with current injection. Interestingly, SC stimulation produces smaller, more facilitating excitatory and IPSCs in KO pyramidal neurons, but larger postsynaptic potentials (PSPs) with the same stimulation. We also found reduced intrinsic firing of parvalbumin (PV)-expressing interneurons and disrupted recruitment of both parvalbumin-expressing and somatostatin (SST)-expressing interneurons in response to patterned synaptic stimulation. Neuronal information processing relies on the interplay between synaptic properties, intrinsic properties that amplify or suppress incoming synaptic signals, and firing properties that produce cellular output. We found changes at each of these levels in *Scn1b* KO pyramidal neurons, resulting in fundamentally altered cellular information processing in the hippocampus that likely contributes to the complex phenotypes of *SCN1B*-linked epileptic encephalopathies.

Key words: Dravet syndrome; encephalopathy; epilepsy; plasticity; *SCN1B*; synaptic integration

Significance Statement

Genetic developmental epileptic encephalopathies have limited treatment options, in part because of our lack of understanding of how genetic changes result in dysfunction at the cellular and circuit levels. *SCN1B* is a gene linked to Dravet syndrome and other developmental epileptic encephalopathies, and *Scn1b* knock-out (KO) mice phenocopy the human disease, allowing us to study underlying neurophysiological changes. Here, we found changes at all levels of neuronal information processing in brains lacking *Scn1b*, including intrinsic excitability, synaptic properties, and synaptic integration, resulting in greatly enhanced input/output functions of the hippocampus. Our study shows that loss of *Scn1b* results in a complex array of cellular and network changes that fundamentally alters information processing in the hippocampus.

Received May 1, 2023; revised Sep. 21, 2023; accepted Oct. 3, 2023.

Author contributions: J.H.C., V.G., and M.A.H. designed research; J.H.C., A.A.A., F.I.G., V.G., and M.A.H. performed research; J.H.C., A.A.A., F.I.G., V.G., and M.A.H. analyzed data; J.H.C. and M.A.H. wrote the first draft of the paper; J.H.C., A.A.A., F.I.G., V.G., and M.A.H. edited the paper; J.H.C. and M.A.H. wrote the paper.

This work was supported by an American Epilepsy Society (AES) Young Investigator award (M.A.H.), an AES Postdoctoral Fellowship (J.H.C.), a Dravet Syndrome Foundation Postdoctoral Fellowship (J.H.C.), a University of Texas at Austin TIDES Undergraduate Research Fellowship (A.A.A.), and the National Institutes of Health/National Institute of Neurological Disorders and Stroke Grant NS112500 (to M.A.H.). This work would not have been possible without the generous gift of the *Scn1b* transgenic mice from Dr. Lori Isom. We thank members of the Howard and Brumback laboratories for helpful discussions, especially our lab managers and technicians who aided in animal care: Mendee Geist, Alexandra Munson, Meredith McCarty, Aurora Weiden, Madelynne Campbell, and Joy Adler.

The authors declare no competing financial interests.

Correspondence should be addressed to MacKenzie A. Howard at mackenziehoward@austin.utexas.edu.

https://doi.org/10.1523/JNEUROSCI.0786-23.2023

Introduction

Neurons extract meaningful information from ongoing neural activity by integrating inputs from thousands of synapses and transforming that information into outputs in the form of action potentials. The amplitude, kinetics, and summation of synaptic potentials is shaped by presynaptic release properties, and postsynaptic ion channels expressed in spine, dendritic, and somatic compartments. The shape and extent of the dendritic arbor, and the relative timing and location of excitatory and inhibitory inputs affect how inputs interact (Spruston, 2008; Kole and Stuart, 2012; Stuart and Spruston, 2015). Thus, information processing by a neural circuit is a finely balanced interplay of many variables, and pathologic disruption of these variables that

alter input/output transformation can result in neurologic disease.

Understanding the full etiology and uncovering therapeutic pathways for neurologic diseases requires defining the causative insult and primary phenotypes, as well as secondary and tertiary effects, including how cellular and circuit processing changes. The variety and complexity of epilepsy disorders illustrate the difficulty of this task. In addition to a wide variety of seizure phenotypes, epilepsy disorders present with a constellation of neuropsychiatric impairments. Symptomology is complex even when the causative insult seems simple in nature (e.g., a single point mutation). Many developmental and epileptic encephalopathies (DEEs) are monogenic disorders that cause drug-resistant seizures and a wide range of cognitive and developmental disabilities (Howard and Baraban, 2017).

Loss-of-function (LOF) *SCN1B* variants result in a range of DEEs, with monoallelic variants resulting in the milder Generalized Epilepsy with Febrile Seizures Plus (GEFS+), and biallelic LOF causing severe early infantile epileptic encephalopathy and Dravet syndrome (Scheffer et al., 2007; Patino et al., 2009; Ogiwara et al., 2012; Aeby et al., 2019). *SCN1B* encodes the protein β1 and the splice variant β1B. β1 was first described as a sodium channel auxiliary subunit (Isom et al., 1992) and modulates the trafficking and physiology of many voltage-gated Na^+ (Hull and Isom, 2018) and K^+ (Marionneau et al., 2012; Nguyen et al., 2012) channels vital for action potential initiation and dendritic excitability. *Scn1b* gene products are also necessary for developmental neuronal patterning, neurite outgrowth, and cell adhesion (Brackenbury et al., 2008, 2013; Patino et al., 2011), and a soluble cleavage product translocates to the nucleus and regulates gene expression (Bouza et al., 2021; Haworth et al., 2022). *Scn1b* is also essential for mature brain function, as deletion in adult mice leads to epilepsy and premature death (O'Malley et al., 2019).

Our goal was to understand how loss of *Scn1b* alters the input/output functions of the hippocampus, using the *Scn1b* knock-out (KO) mouse model, which phenocopies many aspects of *SCN1B* LOF disorders, including spontaneous seizures, ataxia, altered cardiac physiology, developmental delays, and early death (C. Chen et al., 2004; Lopez-Santiago et al., 2007). We measured synaptic integration, synaptic physiology, and intrinsic physiology in CA1 pyramidal neurons and GABAergic interneurons. Rather than a single phenotype that intuitively explains neural dysfunction, we found a constellation of changes to every level of neuronal information processing in the hippocampus. CA1 pyramidal neurons were hyperresponsive to theta burst-patterned synaptic input. We tested hypotheses that this might be because of intrinsic hyperexcitability or increased/unbalanced synaptic strength. We found that while CA1 pyramidal neurons fired more action potentials with current injections, intrinsic physiology changes were complex and implicated multiple ion channel types. Both excitatory and inhibitory synaptic currents were reduced in KO pyramidal cells, but were normally balanced. Finally, we tested the hypothesis that inhibition may be failing to effectively control activity in pyramidal neurons. Parvalbumin-expressing interneurons demonstrated decreased intrinsic firing, and both parvalbumin-expressing and somatostatin (SST)-expressing interneuron subtypes exhibited drastically reduced recruitment in response to theta-burst patterned synaptic input. Thus, the physiological phenotypes associated with loss of *Scn1b* are distributed across cell types and functional domains, and subtle changes to interacting physiological mechanisms combine to alter how synaptic information is processed, likely resulting in the complex etiology of DEEs.

Materials and Methods

Animals

All procedures were approved by the Institutional Animal Care and Use Committee at the University of Texas at Austin. *Scn1b* knock-out mice were a generous gift from Lori Isom at the University of Michigan (C. Chen et al., 2004). The colony was maintained by crossing $Scn1b^{+/-}$ with C57Bl/6J mice (The Jackson Laboratory, strain #000664). To generate experimental mice, we bred $Scn1b^{+/-}$ x $Scn1b^{+/-}$. Male and female $Scn1b^{-/-}$ (KO) and $Scn1b^{+/+}$ [wild-type (WT)] littermates were used for experiments at postnatal day (P)15–P20. To generate interneuron reporter mice, we crossed *Scn1b* knock-out mice with PV-Cre (The Jackson Laboratory, strain #17320) or SST-Cre (The Jackson Laboratory, strain #28864) and the Ai14-TdTomato reporter (The Jackson Laboratory, strain #007914). Pups were toe-clipped at P6–P8 for identification, and tail tissue samples were taken for genotyping by PCR as in C. Chen et al. (2004), or were genotyped by TransnetYX As previously reported, $Scn1b^{-/-}$ mice in our colony had spontaneous seizures and stunted growth beginning around P10 and exhibited 100% mortality by P22 (C. Chen et al., 2004; Hull et al., 2020).

Acute slice preparation

Mice were deeply anesthetized with a mix of ketamine (90 mg/kg; Acor) and xylazine (10 mg/kg; Dechra) intraperitoneally. Mice were transcardially perfused with ice-cold, oxygenated cutting solution, containing (in mM): 205 sucrose, 25 sodium bicarbonate, 2.5 KCl, 1.25 sodium phosphate, 7 $MgCl_2$, 7 D-glucose, 3 sodium pyruvate, 1.3 ascorbic acid, and 0.5 $CaCl_2$. Brains were removed, hemisected, and the dorsal portion of the brain was removed using a scalpel blade, angled at ~20°. The dorsal cut side was then mounted in the slicing chamber of a Leica VT1200 vibratome using superglue, and submerged in ice-cold, oxygenated cutting solution. 250 µm oblique-horizontal hippocampal slices were made. Slices incubated for 30 min at 37°C in holding solution containing (in mM): 125 NaCl, 25 sodium bicarbonate, 2.5 KCl, 1.25 sodium phosphate, 12.5 D-glucose, 2 $MgCl_2$, 2 $CaCl_2$, 1.3 ascorbic acid, and 3 sodium pyruvate. Slices were then stored for at least 30 min, and up to 8 h, in holding solution at room temperature before being used for recordings. Reagents for electrophysiology solutions were purchased from Sigma-Aldrich.

Whole-cell electrophysiology

Slices were transferred to the recording chamber and were continuously bathed in warm (32.5°C), oxygenated artificial cerebrospinal fluid (ACSF), containing (in mM): 125 NaCl, 25 $NaHCO_3$, 2.5 KCl, 1.25 NaH_2PO_4, 12.5 D-glucose, 1 $MgCl_2$, and 2 $CaCl_2$. Only slices from the middle of the dorsal-ventral axis of the hippocampus were used for recordings. Patch pipettes of 3–6 MΩ were pulled from thin-walled borosilicate filamented glass (Sutter BF150-110-10) using a P-1000 puller (Sutter). For current clamp experiments, pipettes were filled with a potassium gluconate solution containing (in mM): 120 K-gluconate, 20 KCl, 10 HEPES, four NaCl, 1 EGTA; 4 Mg-ATP, 0.3 Na-GTP, and 7 phosphocreatine disodium salt hydrate. For voltage clamp experiments, the internal solution contained (in mM): 120 cesium methansulfonate, 4 NaCl, 6 CsCl, 10 HEPES, 1 EGTA, 4 Mg-ATP, 0.3 Na-GTP, 7 phosphocreatine disodium salt hydrate, and 5 QX-314; 0.3% biocytin was included in the internal solution of some experiments for *post hoc* recovery of recorded neurons. Slices were visualized using a Zeiss Axio Examiner with Dodt contrast optics and epifluorescence, and a Zeiss Axiocam 503 infrared digital camera. Data were acquired with a MultiClamp 700B amplifier (Molecular Devices) and an InstruTECH LIH8 + 8 (HEKA) digitizer at a sampling rate of 10 kHz, filtered at 4 kHz (Bessel). Pipette capacitance neutralization and bridge balance were applied, and liquid junction potential was not corrected for. Data were acquired using Axograph software. After measuring resting membrane potential in current clamp experiments, a holding current was applied to give all neurons a baseline membrane potential of ~−70 mV. We excluded cells with a series resistance >25 MΩ or if the series resistance changed by >20% throughout the recording. Synaptic stimulation was delivered by a tungsten bipolar stimulating electrode (WE3ST30.1ASS, Microprobes) placed in the stratum radiatum near the CA2/CA1 border to

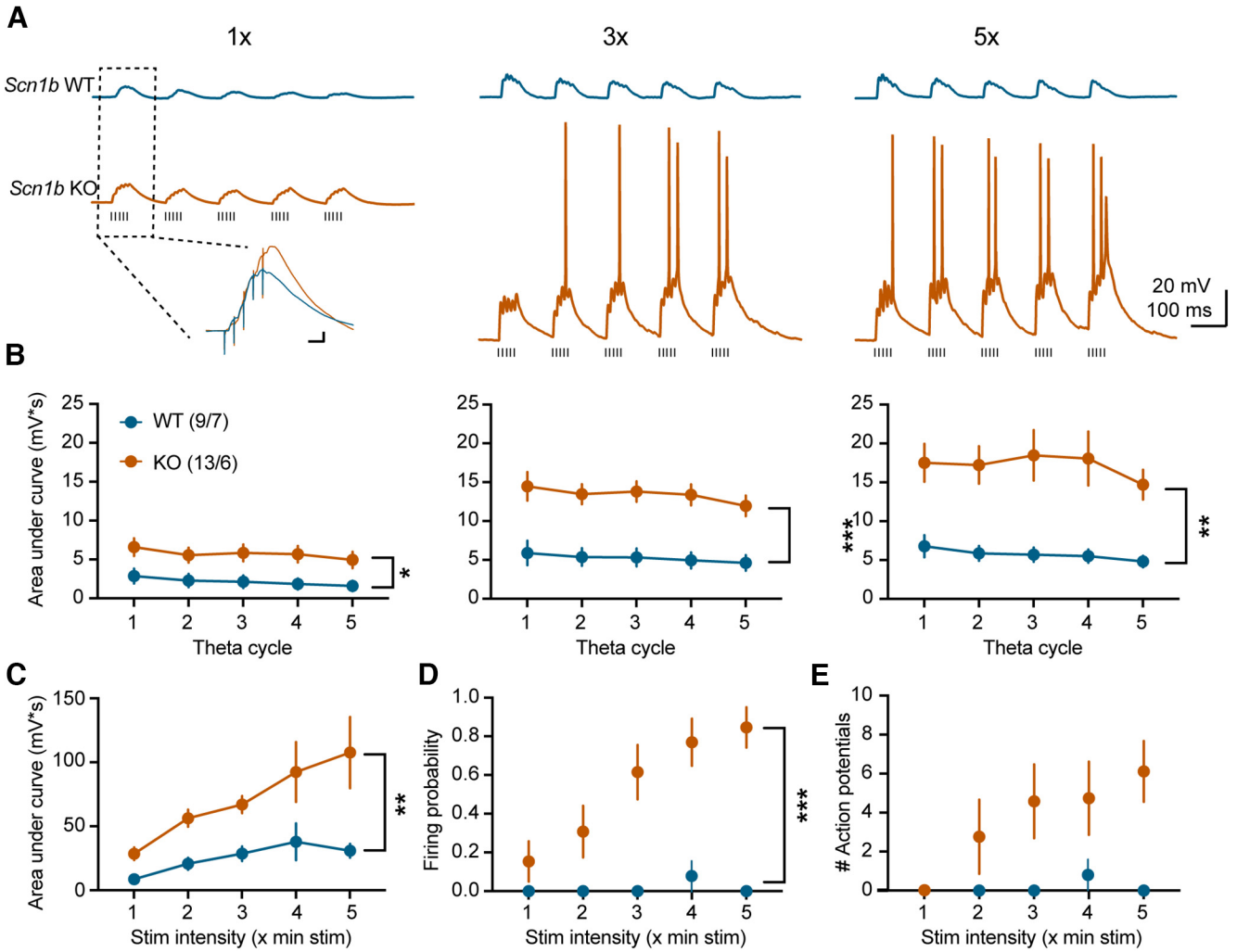

Figure 1. Aberrant temporal summation in *Scn1b* KO CA1 pyramidal neurons. ***A***, Postsynaptic potentials measured in CA1 pyramidal neurons in response to theta burst stimulation of Schaffer collateral axons (5 pulses at 100 Hz, 5 bursts, 200-ms interburst interval; designated by hash marks below traces) from *Scn1b* WT (blue, top) and KO (orange, bottom) neurons. Stim artifacts were removed for clarity. The stimulation intensity was normalized such that the first stimulation of the first burst was 1.5–2 mV. Inset shows expanded view of first theta burst with stim artifacts to demonstrate that the first pulse was the same amplitude across experiments (inset scale = 2 mV, 20 ms). Stimulation intensity was increased by multiples of the minimal stimulus to 3× (middle) and 5× (right). ***B***, At minimal stim intensity (1×; left) *Scn1b* KO neurons had larger responses, i.e., stronger synaptic integration, compared with WT, measured as area under the curve with spikes truncated. As the stimulation intensity was increased, the enhanced integration became more prominent (middle = 3×, right = 5× minimal stim). The amplitude (***C***), firing probability (***D***), and number of action potentials (including 0 s; ***E***) are larger in KO neurons across a range of stimulation intensities in KO neurons compared with WT neurons which did not fire with this stimulation protocol. ***B–D***, *N* = (cells/mice). *$p < 0.05$, **$p < 0.01$, ***$p < 0.001$, main effects of genotype; two-way RM ANOVAs.

stimulate the Schaffer collateral (SC) axons, and a constant current stimulus isolator (World Precision Instruments). Gabazine (GBZ) was purchased from Sigma-Aldrich or Hello Bio. ZD7288 was purchased from Tocris or Hello Bio.

Morphology

Slices containing biocytin filled neurons were fixed in 4% PFA (Electron Microscopy Science) overnight at 4°, and then stored in PBS until processed. Filled neurons were stained using Vectastain ABC-HRP and DAB kits (Vector Labs) and reconstructed using the Neurolucida Tracing Program (MBF Bioscience). Sholl analyses, using a 15-μm radius, were used to measure dendritic length and dendritic branching patterns. Neurons in which major dendritic branches had been cut were excluded from these analyses.

mRNA expression profiling

Mice were anesthetized as above and decapitated. Hippocampi were dissected out and a section of middle hippocampus was isolated and stored in TRIzol reagent (ThermoFisher) at −80°C until processed. Hippocampi sections were crushed using a pestle in the TRIzol reagent and RNA was isolated using manufacturers' recommended protocol. 200 ng of total RNA was reverse transcribed using SuperScript IV First-Strand Synthesis System (Invitrogen) as per the manufacturers' protocol. qPCR was performed with PowerUP SYBR green master mix in ViiA 7 Real-Time PCR System (Applied Biosystems) using fast cycling mode. For data analysis, the average cycle thresholds from five independent biological replicate samples were calculated and normalized to housekeeping control β-*actin*. Primers for each gene analyzed are as follows (forward, reverse): *Hcn1*: CTCAGTCTCTTGCGGTTATTACG, TGGCGAGGTCATAGGTCAT; *Hcn2*: ATCGCATAGGCAAGAAGAACTC, CAATCTCCTGGATGATG GCATT; *Hcn3*: GATGTTTGATGAAGAGAGCATCC, CCCGGCAGG TGAAGTTAATA; *Hcn4*: GCATGATGCTTCTGCTGTGT, GCTTCCC CCAGGAGTTATTC; *Actb*: CTGGCTCCTAGCACCATGAAGATC, TGCTGATCCACATCTGCTGG (Honsa et al., 2014). Relative abundance of the transcripts was calculated using the ΔΔCt method (Livak and Schmittgen, 2001).

Data analysis and statistics

Electrophysiology data were analyzed using Axograph software. Action potentials were counted using the event detection tool in Axograph,

using a fixed amplitude threshold of 0 mV. Spike voltage threshold was defined as the membrane potential where dV/dt reached 10% of the maximum dV/dt. Action potential amplitude was taken as the difference between threshold and max voltage. Input resistance was measured as the slope of the linear portion of current–voltage plot using negative and subthreshold positive current steps. Capacitance was calculated by measuring the time constant (τ) of repolarization from a −50-pA current step and dividing that value by the membrane resistance. Data were analyzed using either Student's *t* tests, Mann–Whitney tests, or ANOVA followed by *post hoc* multiple comparisons tests, as appropriate using GraphPad Prism 9. *N* values used for statistics are number of cells, but number of animals is also listed for each experiment. No more than three cells from a single animal were used for any experiment. For expression profiling, N values are for number of mice. Data are presented as mean ± SEM unless otherwise noted.

Results

Aberrant temporal summation in *Scn1b* KO CA1 pyramidal neurons

A neuron's fundamental role is to receive incoming synaptic inputs, properly filter and integrate those inputs, and produce an appropriate output in the form of action potentials. To examine basic cellular information processing in the hippocampus of *Scn1b* KO mice we performed a synaptic integration study, in which theta burst stimulation (five pulses at 100 Hz per burst, repeated five times at 5 Hz; hash marks below example traces in Fig. 1) was delivered to Schaffer collateral (SC) axons and the resulting postsynaptic voltage response was measured in CA1 pyramidal neurons, a major locus for memory and cognitive processing. Stimulation intensity was normalized to the lowest stimulation that gave a reliable postsynaptic response of 1.5–2 mV for a single stimulation (1×, Fig. 1*A*, left; inset shows an expanded view of the first burst). Using that minimal stimulation intensity, we found that *Scn1b* KO neurons showed enhanced temporal synaptic integration compared with WT littermates, measured as the area under the curve of the voltage response with spikes truncated (Fig. 1*B*, left; Table 1). As we increased the stimulation intensity by multiples of the minimal intensity, the response in KO neurons drastically increased in amplitude (Fig. 1*B*; Table 1). The amplitude of the PSP, probability of firing, and the number of action potentials also increased with stim intensity in KO neurons, whereas this range of stimulation did not drive action potential firing in WT neurons (Fig. 1*C*,*D*; Table 1). This indicates a major shift in input/output processing in CA1 pyramidal neurons lacking *Scn1b*, which intuitively relates to the seizures and changes in cognitive function exhibited by people with *SCN1B*-linked encephalopathies.

Table 1. Theta-stimulation

Figure	Experiment	ANOVA main effects *F* values	*p*
1*B*, left	1× theta stim AUC	Genotype: $F_{(1,20)} = 6.876$	0.016
		Theta cycle: $F_{(1.3,26.4)} = 3.796$	0.052
		Theta cycle × genotype: $F_{(4,80)} = 0.222$	0.925
1*B*, middle	3× theta stim AUC	Genotype: $F_{(1,20)} = 19.3$	0.0003
		Theta cycle: $F_{(1.6,32)} = 2.93$	0.079
		Theta cycle × genotype: $F_{(4,80)} = 0.605$	0.660
1*B*, right	5× theta stim AUC	Genotype: $F_{(1,20)} = 12.89$	0.002
		Theta cycle: $F_{(1.6,33)} = 1.894$	0.172
		Theta cycle × genotype: $F_{(4,80)} = 0.730$	0.574
1*C*	Theta stim vs AUC	Genotype: $F_{(1,20)} = 8.13$	0.009
		Stim intensity: $F_{(2.8,56.17)} = 23.79$	0.014
		Intensity × genotype: $F_{(4,80)} = 1.75$	0.126
1*D*	Firing probability	Genotype: $F_{(1,20)} = 25.3$	<0.0001
		Stim intensity: $F_{(2.8,56.17)} = 7.576$	0.0003
		Intensity × genotype: $F_{(4,80)} = 7.56$	<0.0001
1*E*	Number of APs	Genotype: $F_{(1,20)} = 25.3$	<0.0001
		Stim intensity: $F_{(2.8,56.17)} = 7.576$	0.0003
		Intensity × genotype: $F_{(4,80)} = 7.56$	<0.0001

All comparisons are two-way repeated measures ANOVAs.

Altered intrinsic properties in *Scn1b* null pyramidal neurons

We next tested whether intrinsic firing properties may underly the increased firing shown in Figure 1. Current steps from 0 to 300 pA, in 25-pA increments, 250 ms long, were injected into CA1 pyramidal neurons and firing properties were measured. Indeed, *Scn1b* KO pyramidal neurons fired more action potentials with increasing current injections compared with WT, but only with larger current steps (Fig. 2*A*,*B*; main effect of current step: $F_{(1.6,45.7)} = 115.0$, $p < 0.0001$; genotype: $F_{(1,29)} = 4.736$, $p = 0.037$; current × genotype: $F_{(12,348)} = 3.485$, $p < 0.0001$; two-way RM ANOVA with *post hoc* Sidak's multiple comparisons test). We measured the rheobase (minimum amount of current needed to drive firing) in the cells from Fig. 2*B* and in a second set of cells which were given current steps in 5-pA increments to more accurately assess the rheobase ($n = 10$ WT; 12 KO). These data are combined in Figure 2*C*–*E* because there were no significant differences between experiments. There was no difference in rheobase (Fig. 2*C*; Table 2), threshold voltage of the first action potential (Fig. 2*D*; Table 2) or resting membrane potential between genotypes (Fig. 2*E*; Table 2). However, the amplitude of the first action potential (measured at rheobase) was smaller (Fig. 2*F*; Table 2) and wider, measured as the width at half of the maximum amplitude, in KO pyramidal cells compared with WT (Fig. 2*G*; Table 2).

We next investigated whether the increase in firing of CA1 pyramidal neurons could be attributed to membrane properties. Using a series of negative current steps, we measured passive membrane properties in pyramidal neurons (Fig. 3*A*) and found that at resting membrane potential there was no difference in membrane resistance between WT and KO neurons (Fig. 3*A*; Table 2). The membrane capacitance was lower in KO neurons compared with WT (Fig. 3*B*; Table 2), suggesting that KO neurons may be smaller than WT neurons. Another observation from the negative current steps was that the sag voltage was larger in KO neurons compared with WT (Fig. 3*C*,*D*; Table 2; sag amplitude measured at the smallest hyperpolarizing step in which the neuron reached −90 mV). An increase in voltage sag is an indicator of increased hyperpolarization activated and cyclic-nucleotide-gated (HCN) channel activity. HCN channels are cation channels that open at hyperpolarized potentials, and therefore, decrease membrane resistance and depolarize the membrane. While our measurements showed no change in resting membrane potential (Fig. 2*E*), resting membrane potential is maintained by a complex set of passive and active membrane properties, and other reports have shown that changes in HCN channels in epilepsy models do not necessarily depolarize the membrane at rest (Albertson et al., 2017; Arnold et al., 2019). Increasing HCN activity has been shown to reduce excitability and membrane resistance of pyramidal neurons (Poolos et al., 2002; Fan et al., 2005), whereas downregulation of HCN channels has been linked to hyperexcitability and increased membrane resistance in several epilepsy models (K. Chen et al., 2001; Strauss et al., 2004; Jung et al., 2007). Because there was no difference in membrane resistance (Fig. 3*A*), but lower capacitance (Fig. 3*B*), we hypothesized that *Scn1b* KO CA1 pyramidal neurons may be smaller, which typically correlates with higher membrane resistance, but that increased somatic HCN channels in

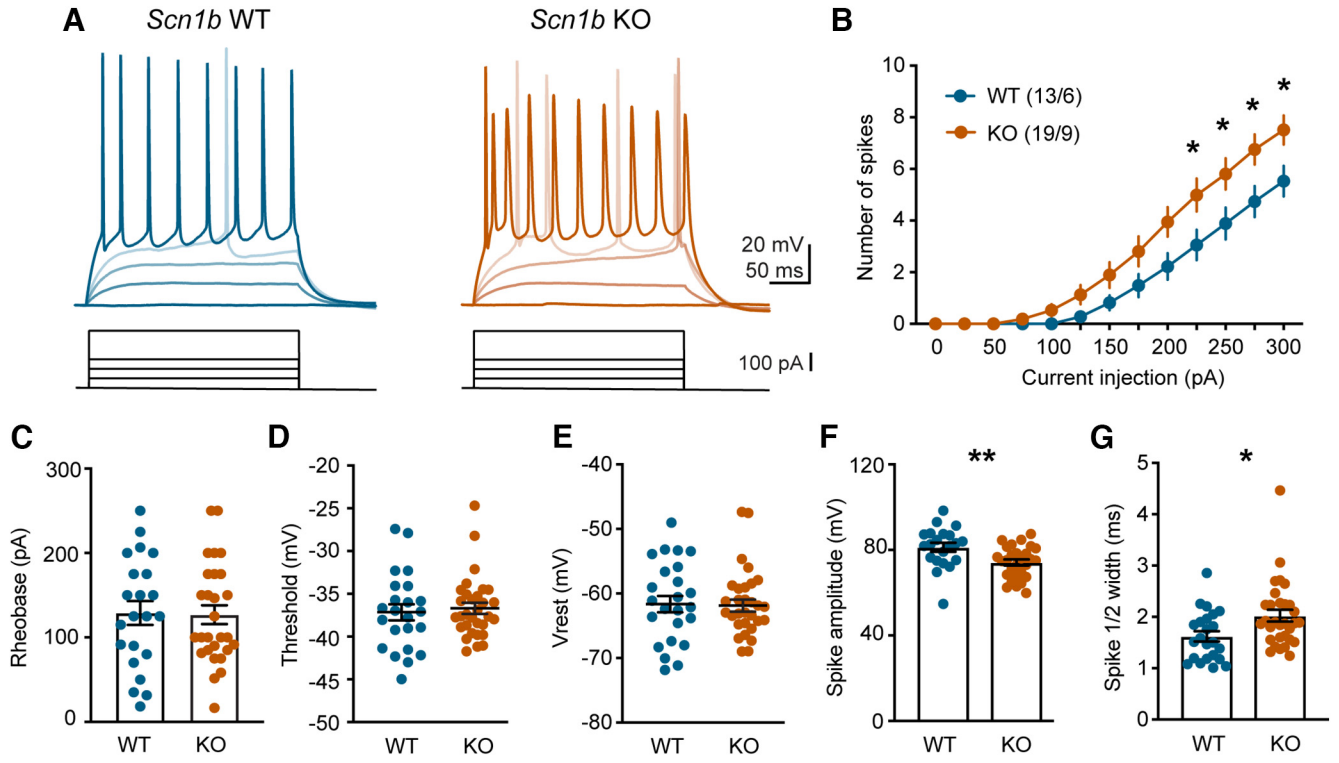

Figure 2. Increased action potential firing in *Scn1b* KO CA1 pyramidal neurons. ***A***, Example voltage responses to increasing current injections from *Scn1b* WT (left, blue) and KO (right, orange) pyramidal cells. ***B***, KO neurons fired more with increasing current injections compared with WT neurons. N = cells/mice. *$p < 0.05$ Sidak's multiple comparisons test. ***C***, KO CA1 pyramidal neurons did not exhibit changes to rheobase, (***D***) threshold voltage, or (***E***) resting membrane potential (Vrest). ***F***, The first action potential (measured at the rheobase current step) had a lower amplitude and (***G***) wider half-width in KO neurons compared with WT. *$p < 0.05$, **$p < 0.01$; t test.

Table 2. Intrinsic properties

Figure	Experiment	WT	KO	t	p
2*C*	Rheobase	130.2 ± 12.5 pA	132.3 ± 9.4 pA	$t_{(52)} = 0.133$	0.894
2*D*	Voltage threshold	−37.3 ± 0.9 mV	−36.8 ± 0.7 mV	$t_{(52)} = 0.425$	0.673
2*E*	Vrest	−61.3 ± 1.3 mV	−61.5 ± 0.9 mV	$t_{(52)} = 0.158$	0.875
2*F*	First spike amplitude	80.33 ± 2.22 mV	73.72 ± 1.30 mV	$t_{(52)} = 2.715$	0.009
2*G*	1/2 width	1.62 ± 0.10 ms	2.02 ± 0.12 ms	$t_{(52)} = 2.528$	0.015
3*A*	Resistance	128.0 ± 19.3 MΩ	KO: 137.4 ± 11.3 MΩ	$t_{(30)} = 0.449$	0.657
3*B*	Capacitance	159.1 ± 12.0 pF	123.4 ± 6.8 pF	$t_{(30)} = 2.775$	0.009
3*D*	Voltage sag	4.56 ± 0.47 mV	5.64 ± 0.19 mV	$t_{(30)} = 2.414$	0.022
3*I*	*Hcn1* ΔΔCT	0.00 ± 0.517	0.178 ± 0.171	$t_{(8)} = 0.327$	0.752
3*I*	*Hcn2* ΔΔCT	0.00 ± 0.174	0.676 ± 0.303	$t_{(8)} = 1.789$	0.112
3*I*	*Hcn3* ΔΔCT	0.00 ± 0.100	−0.080 ± 0.272	$t_{(8)} = 0.275$	0.790
3*I*	*Hcn4* ΔΔCT	0.00 ± 0.182	−0.612 ± 0.283	$t_{(8)} = 1.821$	0.106
4*B*	Total dendritic length	1978 ± 560 µm	1681 ± 793 µm	$t_{(13)} = 0.828$	0.423

All comparisons are unpaired Student's t tests.

KO neurons normalizes the membrane resistance. Indeed, when HCN channels were blocked with the antagonist ZD7288 (20 μM), membrane resistance increased (Fig. 3*E*,*F*; main effect of drug: $F_{(1,29)} = 11.06$, $p = 0.002$), and the increase was larger in KO neurons compared with WT (genotype × drug: $F_{(1,29)} = 4.277$, $p = 0.048$); genotype: $F_{(1,29)} = 2.007$, $p = 0.167$; two-way RM ANOVA). ZD7288 significantly increased the resistance of KO neurons ($p = 0.032$, Sidak's multiple comparisons test), but not WT neurons ($p = 0.994$), consistent with previous data showing that wild-type CA1 pyramidal cells have few HCN channels at the soma (Magee, 1998). Sag voltages were larger in KO neurons, but ZD7288 similarly blocked sag in both genotypes (Fig. 3*E*; WT: 87.37 ± 3.12% block; KO: 74.81 ± 6.09%; $p = 0.545$, Mann–Whitney test; summary data not shown). To further test this hypothesis, we measured membrane resistance while varying the membrane potential, and found an increased slope in the KO data when resistance is plotted against membrane potential (Fig. 3*G*,*H*; main effect of voltage: $F_{(1.77,35.4)} = 121.1$, $p < 0.0001$; genotype: $F_{(1,20)} = 0.292$, $p = 0.595$; voltage × genotype: $F_{(4,80)} = 4.569$, $p = 0.02$; two-way RM ANOVA), suggesting that membrane resistance increases more in KO neurons as the cell depolarizes and HCN channels deactivate. These data together suggest that *Scn1b* KO CA1 pyramidal neurons likely have more compact somata than WT, but somatic HCN channel number or activity is increased, normalizing the input resistance and rheobase. However, at more depolarized potentials, where HCN channels are deactivated, KO neurons exhibit increased excitability (Fig. 2*B*, current steps > 200 pA).

To understand whether these changes in HCN channel function were associated with changes in gene expression, we isolated hippocampi from WT and *Scn1b* KO mice for expression profiling. We measured mRNA abundance for each member of the HCN channel family, normalizing data to mRNA for β-actin (*Actb*). We found that none of the four HCN genes exhibited significantly different expression levels in *Scn1b* KO hippocampi compared with WT (Fig. 3*I*; Table 2). We also plotted abundance of each family member relative to *Hcn1*. As shown previously (Moosmang et al., 1999; Surges et al., 2006; Dougherty et al., 2013), the dominant HCN gene expressed in hippocampus was *Hcn1*, with intermediate levels of *Hcn2*, and much lower levels of Hcn3 and Hcn4 (Fig. 3*J*). These experiments used whole hippocampus rather than isolating CA1 pyramidal neurons, so come with the caveat that changes in expression in that specific cell type may be diluted.

Overall, our intrinsic physiology data indicate modest hyperexcitability in these neurons, but the mixed changes in somatic membrane properties, lack of change to rheobase, threshold, or

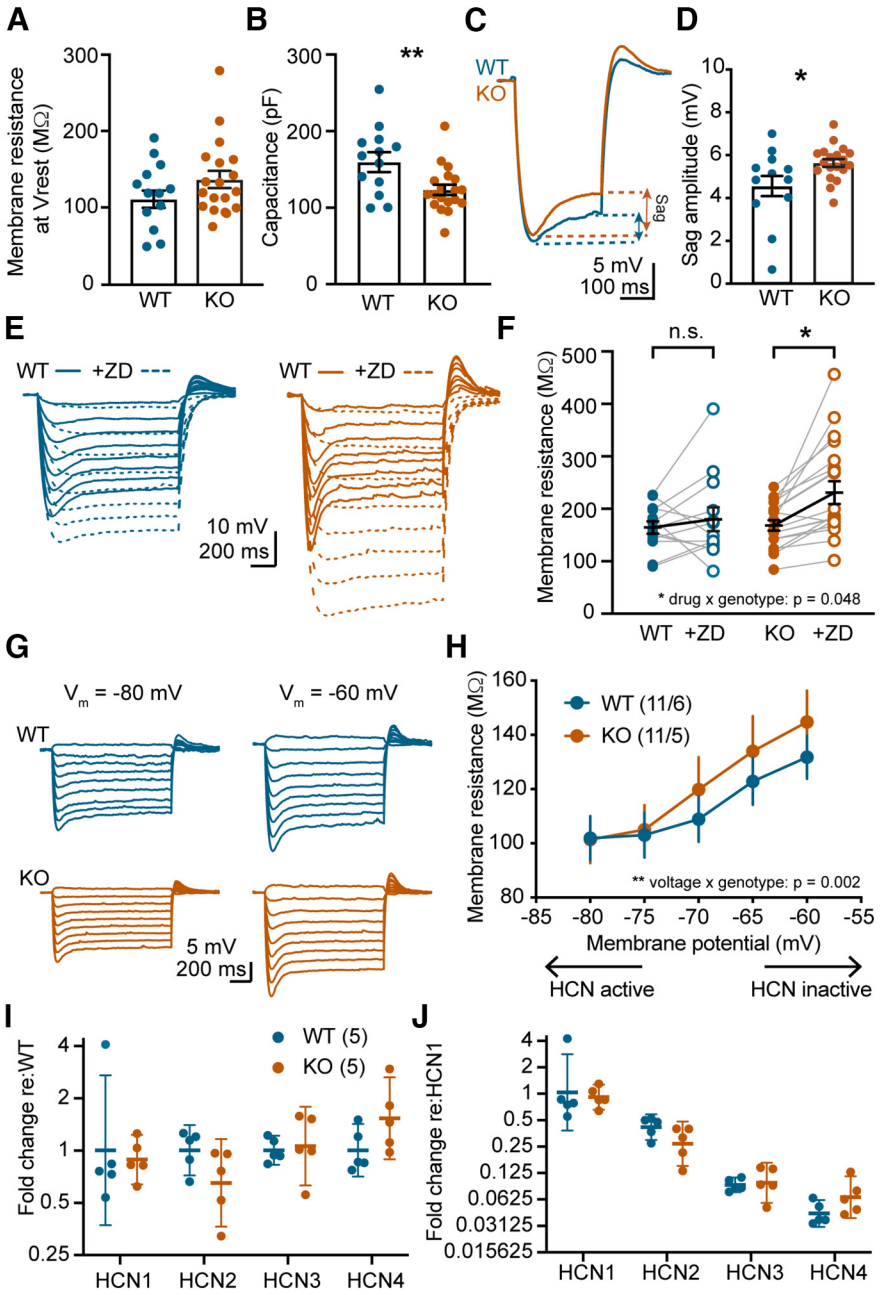

Figure 3. Increased HCN activity normalizes membrane resistance in *Scn1b* KO pyramidal neurons. ***A***, Membrane resistance was not different, while capacitance (***B***) was decreased in KO pyramidal cells compared with WT at resting membrane potential. $^{**}p < 0.01$, *t* test. ***C***, Example voltage traces of a hyperpolarizing current step to −90 mV from a WT (blue) and KO (orange) pyramidal cell. Sag amplitude = peak negative voltage − steady state voltage. ***D***, KO neurons show greater mean sag amplitude to current steps that cause peak hyperpolarization to −90 mV. $^{*}p < 0.05$, *t* test. ***E***, Example voltage responses to hyperpolarizing current steps (−10 to −150 pA, 20-pA increments, 1 s) from WT (left, blue) and KO (right, orange) pyramidal cells in the absence (solid lines) and presence of 20 μM ZD7288 (dashed lines). ***F***, Blockade of HCN channels with ZD7288 has a larger effect on membrane resistance of KO neurons compared with WT. $N = 12$ cells from 5 mice WT, 18 cells from 10 mice KO. n.s. = not significant ($p > 0.05$), $^{*}p < 0.05$, Sidak's multiple comparisons test. ***G***, Example voltage traces in response to currents steps (+10 to −150 pA, 20-pA increments, 1 s) while holding the cell at varying membrane potentials (left = −80 mV; right = −60 mV). ***H***, Summary data of membrane resistance versus membrane potential. $N =$ (cells/mice). ***I***, mRNA expression levels of HCN genes in WT and KO hippocampi normalized to WT. Bars indicate geometric mean, error bars indicate 95% confidence intervals, $N =$ mice. ***J***, Geometric mean (±95% confidence intervals) of mRNA expression data normalized to WT *Hcn1*.

action potential number in response to smaller suprathreshold steps were surprising given the large increases in the input/output function to synaptic stimulation.

A previous study found that increased excitability was associated with reduced dendritic arborization in subicular pyramidal neurons expressing a pathogenic *Scn1b* variant (Reid et al., 2014). Furthermore, *Scn1b* KO mice have deficits in neurite outgrowth (Brackenbury et al., 2008). As such, we hypothesized that the decreased capacitance and hyperexcitability in *Scn1b* knockout CA1 pyramidal neurons could be due in part to reduced dendritic arborization. Recorded neurons were filled with biocytin and reconstructed. CA1 pyramidal cell dendritic structures are highly variable at this early age, as revealed by WT and KO neuron reconstructions (Fig. 4*A*). There was no difference in total dendritic length (Fig. 4*B*; Table 2), or number of crossings as a function of distance from the soma between genotypes (Fig. 4*C*; main effect of Sholl radius: $F_{(65,849)} = 15.83$, $p < 0.0001$; main effect of genotype: $F_{(1,849)} = 3.415$, $p = 0.065$; genotype × radius:

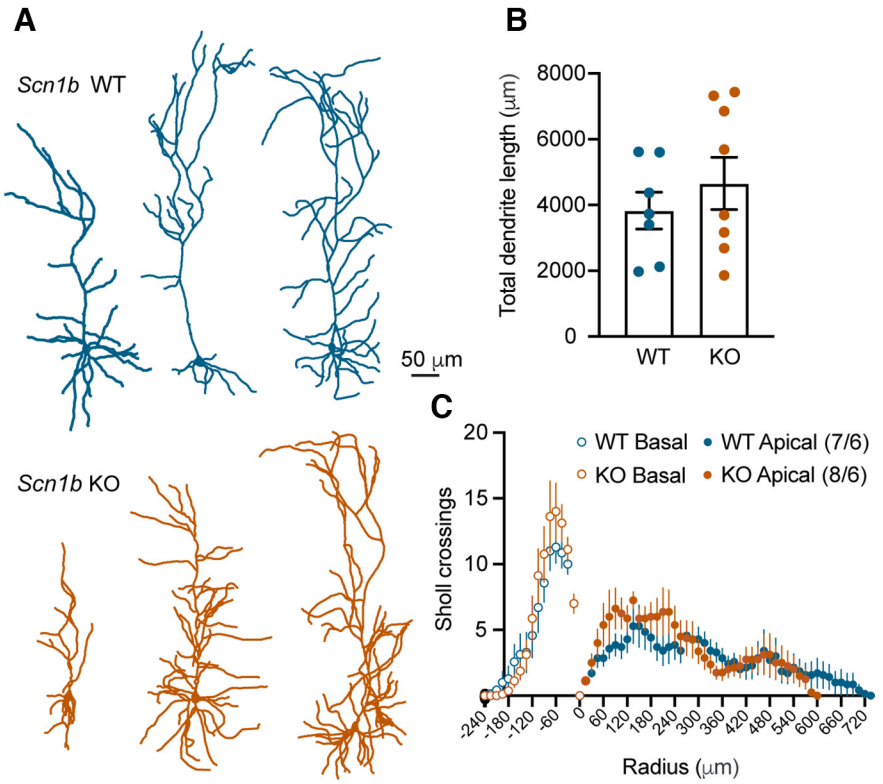

Figure 4. No change in dendritic structure in KO pyramidal neurons. ***A***, Example reconstructions of *Scn1b* WT (top, blue) and KO (bottom, orange) CA1 pyramidal neurons. ***B***, No difference in total dendrite length between genotypes. ***C***, No difference in number of Sholl crossings using 15-μm radii for apical (solid circles) or basal dendrites (open circles). *N* = (cells/mice).

$F_{(65,849)} = 0.774$, $p = 0.904$; two-way ANOVA). These data indicate that the enhancement in excitability and synaptic integration were not associated with gross changes in dendritic morphology.

Altered synaptic inputs in *Scn1b* null hippocampus

The subtle differences in KO intrinsic excitability described above are unlikely to fully account for the dramatic increase in synaptic integration seen in Figure 1. We next tested the hypothesis that excitatory synaptic inputs to *Scn1b* KO neurons were enhanced, or the balance of excitation and inhibition was altered. First, we used voltage clamp to isolate EPSCs by holding the membrane at the reversal potential for GABA (−70 mV). We stimulated the SCs, normalizing to the lowest stimulation intensity that reliably evoked a postsynaptic current (~40 pA EPSC in both genotypes), and then increased the intensity by multiples of that threshold to generate an input/output curve. Counter to expectations following current clamp experiments, the growth curve of the EPSC input/output curve was significantly lower in *Scn1b* KO neurons compared with WT (Fig. 5*A*,*B*; Table 3). The same neurons were then clamped at +10 mV to isolate IPSCs (IPSCs), and using the same stimulation intensities as in Figure 5*B*, we found that the IPSCs were also substantially smaller in KO neurons compared with WT (Fig. 2*A*,*C*; Table 3). There was no change in PSC kinetics between genotypes (Table 4). While both EPSCs and IPSCs were smaller in KO neurons, they were also more facilitating, measured as an increase in paired-pulse ratio (Fig. 5*A*,*D*; Table 4). EPSCs and IPSCs scaled down in a similar manner, as there was no difference in excitatory to inhibitory ratio between genotypes (Fig. 5*E*; Table 3). We next measured spontaneous synaptic events, and found no difference in the frequency or amplitude of sEPSCs or sIPSCs (Fig. 5*F*–*K*; Table 4). Finding significantly smaller PSCs, and a lack of difference in excitatory to inhibitory ratio, with unchanged spontaneous synaptic events was unexpected given the significantly larger temporal synaptic integration seen in Figure 1.

We next performed a similar input/output experiment in current clamp to measure SC driven postsynaptic potentials (PSPs). We used a single input stimulation paradigm similar to that in Figure 5, which produced smaller synaptic current growth functions in KO neurons, and again normalized stim intensity to the lowest suprathreshold intensity that evoked a reliable postsynaptic potential (~ 1 mV in amplitude), then increased by multiples of that threshold stimulation. No synaptic blockers were present to measure a mixed PSP. KO neurons had larger PSPs (APs excluded/truncated) compared with WT (Fig. 6*A*,*B*; Table 3). We also found that a proportion of KO cells fire with a single stimulation, whereas WT neurons do not. However, the firing probability was not significantly different between genotypes (Fig. 6*C*; Table 3).

While our voltage clamp experiments revealed similar excitatory/inhibitory ratios between genotypes (Fig. 5*E*), altered interactions between these inputs could underlie the larger synaptic depolarizations in *Scn1b* KO pyramidal neurons in current clamp. We hypothesized that if the enhanced postsynaptic potentials were because of a reduction in inhibitory control of synaptic integration, blocking inhibition would have a larger effect on WT neurons compared with KOs. We washed on the $GABA_A$ antagonist gabazine (10 μM, GBZ; Fig. 6*A*), and found that while responses in both genotypes were increased, gabazine increased the amplitude (Fig. 6*D*) and spiking (Fig. 6*E*; Table 3) of KO neurons to a greater extent. This is contrary to our hypothesis of functionally deficient inhibition, suggesting that GABAergic inhibition is controlling a much greater degree of hyperexcitability to synaptic input in the *Scn1b* null hippocampus. However, this

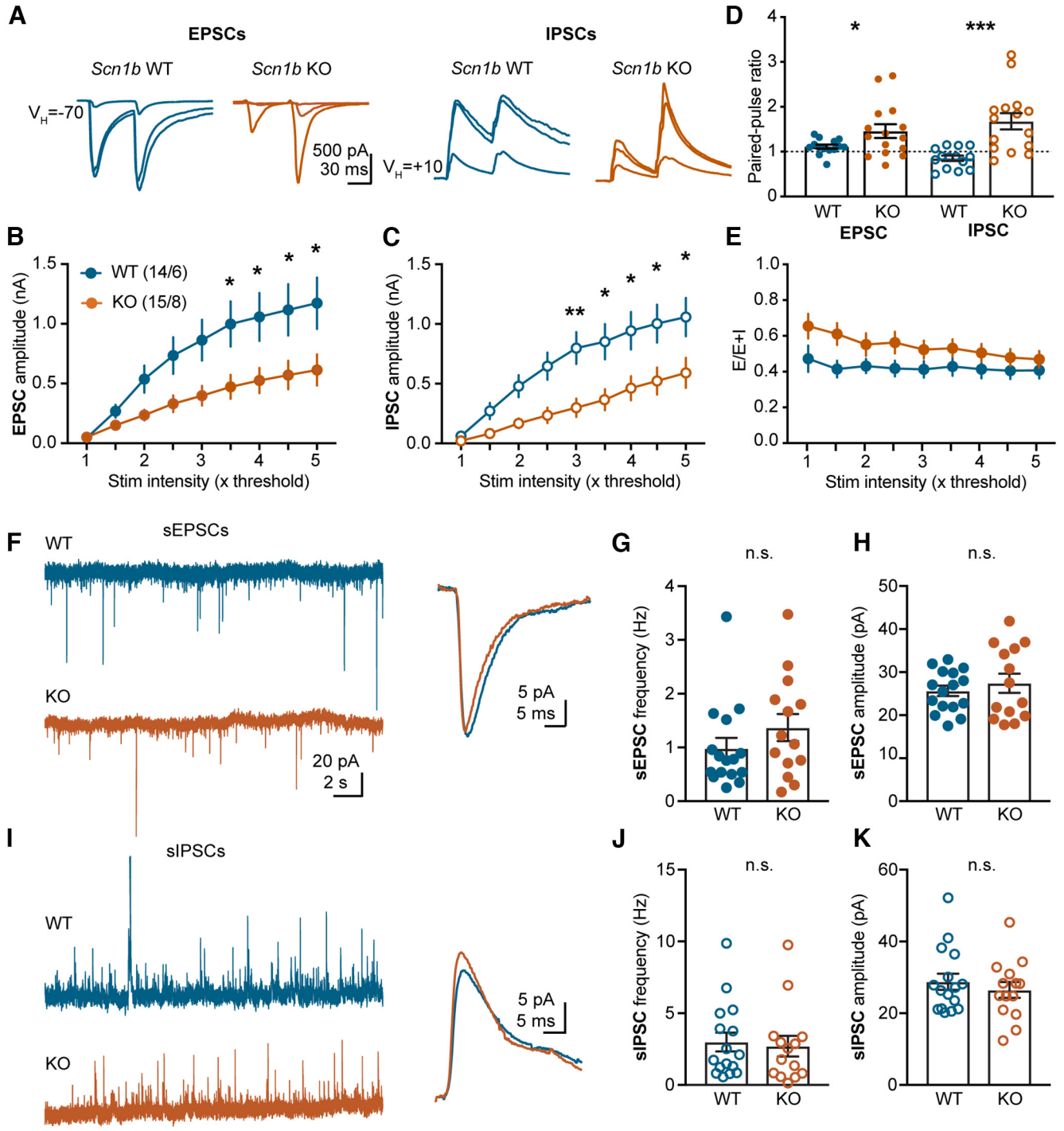

Figure 5. Smaller synaptic currents in *Scn1b* KO pyramidal neurons. ***A***, Example whole-cell voltage clamp recording responses to paired Schaffer collateral stimulation (50-ms interstimulus interval) at one, three, and five times (overlayed) the minimal stimulation intensity necessary to evoke a reliable EPSC. EPSCs were recorded by voltage-clamping the cell E_{GABA} (−70 mV) and IPSCs at $E_{glutamate}$ (+10 mV). ***B***, Summary data of EPSC input/output curve demonstrates that EPSCs were smaller across stimulation intensities in KO neurons compared with WT. N = cells/mice. ***C***, Summary data of IPSC input/output showing that IPSCs were also smaller in KO neurons ($^*p < 0.05$, $^{**}p < 0.01$, Sidak's multiple comparisons test). ***D***, Increased paired-pulse ratio of both EPSCs (left, closed circles) and IPSCs (right, open circles) in KO neurons at 3× stim intensity. $^*p < 0.05$, $^{***}p < 0.001$, Mann–Whitney tests. ***E***, Summary data of excitatory to inhibitory ratio, measured as the area of the EPSC/(EPSC + IPSC). ***F***, Example spontaneous EPSCs (sEPSCs) recorded at E_{GABA} (−70 mV; left) from *Scn1b* WT (top, blue) and KO (bottom, orange) pyramidal neurons. Right, Averaged WT and KO sEPSCs overlaid. ***G***, No difference in frequency or (***H***) amplitudes of sEPSCs between WT and KOs (n.s. = $p > 0.05$; t tests). ***I***, Example spontaneous IPSCs (sIPSCs) recorded at $E_{glutamate}$ (+10 mV). ***J***, No difference in frequency or (***K***) amplitude of sIPSCs between WT and KOs (n.s. = $p > 0.05$; t tests).

is a single stimulation, and the enhanced synaptic integration seen in Figure 1 could be driven by a breakdown of GABAergic signaling with high frequency stimulation.

To address the role of inhibition in synaptic integration, we repeated the theta burst paradigm in a new set of cells. We again normalized the stimulation intensity such that the first stimulation elicited a consistent PSP of 1–2 mV (as in Fig. 1), measured temporal integration of theta burst stimulation in standard ACSF, and then washed on gabazine (10 μM; Fig. 6*F*). We again found that the postsynaptic responses were larger in *Scn1b* KO

Table 3. Synaptic transmission

Figure	Experiment	ANOVA main effects	Test
5*B*	Evoked EPSCs	Stim intensity: $F_{(8,216)} = 36.38$, $p < 0.0001$ Genotype: $F_{(1,27)} = 6.082$, $p = 0.020$ Stim intensity × genotype: $F_{(8,216)} = 4.382$, $p < 0.0001$	Two-way RM ANOVA
5*C*	Evoked IPSCs	Stim intensity: $F_{(8,216)} = 46.32$, $p < 0.0001$ Genotype: $F_{(1,27)} = 8.648$, $p = 0.007$ Stim intensity × genotype: $F_{(8,216)} = 44.226$, $p < 0.0001$	Two-way RM ANOVA
5*E*	E/I ratio	Stim intensity: $F_{(8,216)} = 3.613$, $p = 0.0006$ Genotype: $F_{(1,27)} = 3.371$, $p = 0.077$ Stim intensity × genotype: $F_{(8,216)} = 1.297$, $p = 0.246$	Two-way RM ANOVA
6*B*	PSP amplitude	Intensity: $F_{(8,216)} = 48.380$, $p < 0.0001$ Genotype: $F_{(1,27)} = 6.476$, $p = 0.017$ Stim intensity × genotype: $F_{(8,216)} = 2.301$, $p = 0.022$	Two-way RM ANOVA
6*C*	Firing probability	Stim intensity: $F_{(8,216)} = 1.922$, $p = 0.058$ Genotype: $F_{(1,27)} = 2.300$, $p = 0.141$ Stim intensity × genotype: $F_{(8,216)} = 1.922$, $p = 0.058$	Two-way RM ANOVA
6*D*	AUC out and in GBZ	Stim intensity: $F_{(8,216)} = 6.777$, $p < 0.0001$ Drug: $F_{(1,27)} = 50.10$, $p < 0.0001$ Genotype: $F_{(1,27)} = 6.469$, $p = 0.017$ Stim intensity × drug: $F_{(8,216)} = 3.284$, $p = 0.002$ Stim intensity × genotype: $F_{(8,216)} = 1.379$, $p = 0.207$ Drug × genotype: $F_{(1,27)} = 4.856$, $p = 0.036$ Stim intensity × drug × genotype: $F_{(8,216)} = 0.876$, $p = 0.538$	Three-way RM ANOVA
6*E*	Spikes in GBZ	Stim intensity: $F_{(8,216)} = 4.216$, $p = 0.0001$ Genotype: $F_{(1,27)} = 3.370$, $p = 0.077$ Intensity × genotype: $F_{(8,216)} = 2.568$, $p = 0.0107$	Two-way RM ANOVA
6*G*	AUC theta stim out and in GBZ	Genotype: $F_{(1,45)} = 26.59$, $p < 0.0001$ Drug: $F_{(1,45)} = 221.5$, $p < 0.0001$ Theta cycle: $F_{(4,116)} = 4.774$, $p = 0.001$ Drug × genotype interaction ($F_{(1,29)} = 7.945$, $p = 0.009$ Theta cycle × genotype: $F_{(1,116)} = 0.694$, $p = 0.598$ Theta cycle × drug: $F_{(4,116)} = 6.926$, $p < 0.0001$ Theta cycle × genotype × drug: $F_{(1,116)} = 1.182$, $p = 0.322$	Three-way RM ANOVA
6*H*	Theta stim #APs out and in GBZ	Drug: $F_{(1,58)} = 19.03$, $p < 0.0001$ Genotype: $F_{(1,58)} = 6.155$, $p = 0.016$ Drug × genotype: $F_{(1,58)} = 1.514$, $p = 0.224$	Two-way ANOVA
6*J*	Theta stim with QX-314 out and in GBZ	Stim intensity: $F_{(1.87,33.7)} = 41.87$, $p < 0.001$ Genotype: $F_{(1,18)} = 0.26$, $p = 0.61$ Intensity × genotype: $F_{(4,72)} = 1.296$, $p = 0.280$	Two-way RM ANOVA

Table 4. Synaptic properties

Figure	Experiment	WT	KO	Statistics	*p*	Test
5*A*	EPSC rise	3.323 ± 0.327 ms	3.352 ± 0.403	$t_{(31)} = 0.038$	0.97	Student's *t* test
5*A*	EPSC decay τ	9.867 ± 0.600 ms	8.140 ± 1.106 ms	$t_{(31)} = 1.435$	0.161	Student's *t* test
5*A*	IPSC rise	4.032 ± 0.491 ms	4.218 ± 0.627 ms	$t_{(31)} = 0.238$	0.814	Student's *t* test
5*A*	IPSC decay τ	27.700 ± 2.202 ms	19.390 ± 3.287 ms	$t_{(31)} = 1.382$	0.177	Student's *t* test
5*D*	EPSC PPR	1.052 ± 0.066	1.599 ± 0.281	$U = 63$	0.046	Mann–Whitney
5*D*	IPSC PPR	0.803 ± 0.102	1.699 ± 0.471	$U = 31$	0.0008	Mann–Whitney
5G	sEPSC frequency	0.981 ± 0.198 Hz	1.370 ± 0.253 Hz	$t_{(28)} = 1.27$	0.23	Student's *t* test
5*H*	sEPSC amplitude	17.54 ± 1.21 pA	17.77 ± 2.24 pA	$t_{(28)} = 0.716$	0.48	Student's *t* test
5*J*	sIPSC frequency	2.992 ± 0.655 Hz	2.701 ± 0.721 Hz	$t_{(28)} = 0.299$	0.767	Student's *t* test
5*K*	sIPSC amplitude	28.77 ± 2.25 pA	26.50 ± 2.22 pA	$t_{(28)} = 0.716$	0.48	Student's *t* test

neurons compared with WT (Fig. 6*G*, main effect of genotype: $p < 0.0001$; Table 3) and that gabazine increased this response (main effect of drug: $p < 0.0001$). As with responses to single stimuli, KO neurons showed a much greater increase in activation with inhibition removed than did WT, as revealed by a significant drug × genotype interaction ($p = 0.009$; Table 3). Blocking GABA also increased firing in response to theta burst stimulation of SC axons (Fig. 3*H*; Table 3; main effect of drug: $p < 0.0001$), and KO neurons fired more action potentials than WT neurons (main effect of genotype: $p = 0.016$), but GABA blockade did not differentially affect one genotype over the other (drug × genotype: $p = 0.224$; Table 3). In summary, both single and patterned stimulation evoked large, long-lasting PSPs and repetitive firing in *Scn1b* KO slices when $GABA_A$ signaling was blocked, indicating that GABA effectively dampens runaway excitability in the KO hippocampus.

The surprising result that PSPs were larger in *Scn1b* null neurons despite smaller synaptic currents suggests that alterations in membrane properties enhance synaptic integration. While we have shown a modest enhancement in membrane resistance at depolarized potentials, this is cannot fully explain the robust enhancement in synaptic integration found in *Scn1b* KO

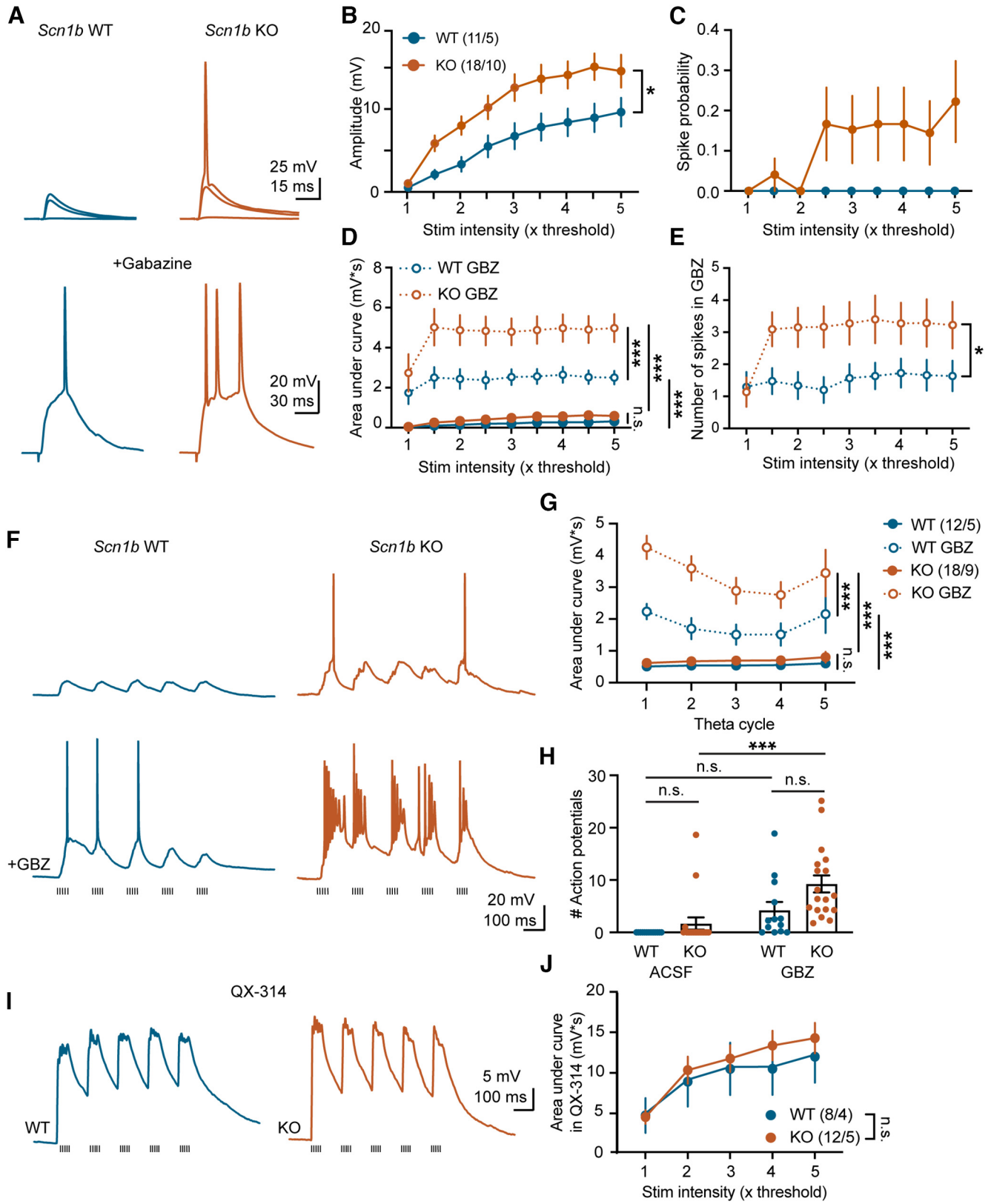

Figure 6. Larger postsynaptic potentials in *Scn1b* KO pyramidal neurons. ***A***, Example current clamp recordings of postsynaptic potentials in response to Schaffer collateral stimulation at one, three, and five times the threshold intensity from WT (left, blue) and KO (right, orange) neurons with GABAergic signaling intact (top). Bottom traces are with $GABA_A$ signaling blocked with gabazine (GBZ; 10 μm; 3× threshold stim). ***B***, Summary input/output data showing that mixed postsynaptic potentials are larger in KO neurons compared with WT. N = cells/mice. *$p = 0.017$ for main effect of genotype, two-way RM ANOVA. ***C***, Spike probability versus stim intensity for WT and KO neurons when GABA signaling is intact demonstrating that some KO neurons begin to fire with a single stimulation, and WT neurons do not. ***D***, Amplitude of PSPs, measured as area under the curve with spikes truncated. Solid circles are mixed PSPs. Open circles are in presence of gabazine. ***$p < 0.001$; n.s. = not significant ($p > 0.05$), Tukey's multiple comparisons tests. ***E***, Number of spikes versus stim intensity in gabazine. *$p < 0.05$ main effect of genotype, two-way RM ANOVA. ***F***, Example traces from *Scn1b* WT (left) or KO (right) neurons in response to theta burst stimulation of Schaffer collaterals (5 pulses at 100 Hz, repeated 5

neurons. We next tested whether active membrane properties contribute to the enhanced synaptic integration by repeating the theta-burst stimulation paradigm in another set of pyramidal neurons in which we included QX-314 (5 mM) in the intracellular solution. QX-314 is a potent voltage-gated sodium channel blocker (Isaac and Wheal, 1993), but has also been shown to block or reduce voltage-gated Ca^{2+} currents (Talbot and Sayer, 1996), hyperpolarization-activated cation currents (Ih; Perkins and Wong, 1995), and K^+ currents (Oda et al., 1992), effectively eliminating active membrane conductances responsible for the enhancement and propagation of signals in pyramidal neurons. In the presence of QX-314, we found no difference in the magnitude of theta-burst driven PSPs between WT and KO neurons across a range of stimulation intensities (Fig. 6*I*,*J*; Table 3). These data indicate that enhanced synaptic integration in *Scn1b* KO neurons requires active conductances.

Disrupted interneuron recruitment in *Scn1b* null mice

Because of the recurrent/epileptiform activity in KO slices in gabazine (Fig. 6*A*,*F*), pharmacological GABA blockade is not a feasible way to effectively test the role of inhibition in synaptic in processing of inputs. Previous studies have reported mixed results on how *Scn1b* deficits alter the excitability of GABAergic interneurons (Reid et al., 2014; Hull et al., 2020), and none have examined the recruitment of interneurons during physiologically relevant synaptic stimulation. We focused on two major hippocampal interneuron populations in CA1, parvalbumin (PV+)-expressing fast-spiking interneurons that mainly provide feedforward inhibition to the soma or perisomatic regions to regulate pyramidal cell firing, and somatostatin (SST+)-expressing interneurons located in stratum oriens, that provide mostly feedback inhibition to the dendrites of pyramidal neurons to regulate synaptic integration (Pelkey et al., 2017). We crossed the *Scn1b* knock-out mouse line with PV-Cre-Ai14-TdTomato and SST-Cre- Ai14-TdTomato reporter mice to identify interneurons in hippocampal slices.

Using a series of current steps, we measured firing properties of CA1 PV+ interneurons (Fig. 7*A*) and found that fast-spiking PV+ neurons from KO slices fired fewer action potentials compared with WT (Fig. 7*B*; Table 5). The mechanism for this change in firing is not immediately clear as it was not accompanied by a change in resting membrane potential (Fig. 7*C*; $t_{(43)} = 0.744$; $p = 0.461$; *t* test), membrane resistance (Fig. 7*D*; $t_{(43)} = 0.556$ $p = 0.581$; *t* test), voltage threshold (Fig. 7*E*, left; $t_{(43)} = 0.873$; $p = 0.388$; *t* test), or rheobase (Fig. 7*E*, right; $t_{(43)} = 1.211$; $p = 0.236$; *t* test). We also found no difference in capacitance of PV+ cells between genotypes (not shown; WT: 134.1 ± 8.890 pF; KO: 134.8 ± 10.91 pF; $t_{(43)} = 0.050$, $p = 0.960$). In contrast, firing properties of SST+ interneurons were not different between genotypes (Fig. 7*F*,*G*; Table 5). We also found no change in resting membrane potential (Fig. 7*H*; $p = 0.663$; Mann–Whitney test), membrane resistance (Fig. 7*I*; $t_{(51)} = 1.536$ $p = 0.131$; *t* test), voltage threshold (Fig. 7*J*, left; $t_{(51)} = 0.848$; $p = 0.400$; *t* test), or rheobase between genotypes (Fig. 7*J*, right; $t_{(51)} = 1.728$; $p = 0.090$; *t* test).

We next tested how these interneuron subtypes are recruited during theta-burst stimulation of stratum radiatum. Like CA1 pyramidal neurons, many CA1 PV+ interneurons receive direct excitation from Schaffer collateral axons, as well as feedforward inhibition. In response to theta-burst stimulation, WT and KO PV+ interneurons had similar responses at the minimal stimulation intensity (Fig. 8*A*,*B*; Table 5). As stim intensity was increased as in earlier experiments, PV+ cells from KO mice displayed smaller PSPs (avg AUC at 5× stim: WT = 7514 ± 1112 mv*ms; KO = 4378 ± 832.2 mv*ms; $t_{(22)} = 2.258$, $p = 0.034$, *t* test) and fired fewer action potentials than those from WT mice (Fig. 8*A*,*B*; Table 5). These data suggests that PV+ interneurons are less excitable and much less likely to be recruited during physiological activity, and a reduction in fast (peri)somatic inhibition may contribute to the increased integration and firing in KO pyramidal neurons seen in Figure 1.

We also investigated the recruitment of SST+ interneurons by theta-burst stimulation. Because these cells receive excitatory synaptic input from CA1 pyramidal neurons (Müller and Remy, 2014) and their measured intrinsic properties were normal, we hypothesized that the increased firing of KO pyramidal neurons (Fig. 1) would increase the recruitment of SST+ interneurons, possibly providing strong inhibitory control although inhibitory synaptic inputs onto pyramidal neurons were diminished in amplitude. We again performed the theta-burst stimulation paradigm in stratum radiatum while recording from SST-Cre-TdTomato+ neurons in stratum oriens from *Scn1b* WT and KO mice (Fig. 8*C*). Unexpectedly, we found that despite normal intrinsic firing properties, recruitment of SST+ neurons was greatly diminished in KO mice, firing fewer action potentials than those from WT mice across all stimulation intensities (Fig. 8*A*,*B*; Table 5). Because these cells provide inhibition to the dendrites of CA1 pyramidal neurons to regulate synaptic integration, the lack of recruitment of SST+ neurons may contribute to the enhanced synaptic integration in pyramidal neurons.

Overall, our results demonstrate dysfunction at multiple levels of neuronal processing (synaptic properties, intrinsic excitability, synaptic integration, interneuron recruitment) that interact to change how the circuit processes ongoing activity. While some of these changes are unexpected or counterintuitive, the complex neurophysiological changes following *Scn1b* loss provide insight into why DEEs are such complex disorders that are often unresponsive to current antiseizure medications.

Discussion

Our data reveal that loss of *Scn1b*, a causative gene for DEEs, alters subthreshold and suprathreshold intrinsic properties, excitatory and inhibitory synaptic physiology, and synaptic integration that were not restricted to a single neuron type or consistent across cell types. The result is a dramatic increase in the input/output function of hippocampal CA1 pyramidal neurons, a key hub for information processing and memory formation. This likely underlies the myriad neurologic deficits experienced even in interictal periods by people suffering from these disorders.

The known biochemistry of *Scn1b* gene products provides interesting clues toward, but not a complete explanation of our complex results. While *SCN1B* was identified and named for its

←

times, 200-ms interburst interval; hash marks below) in standard ACSF (top) or gabazine (10 μm; bottom). ***G***, Magnitude of temporally summed PSPs, measured as area under the curve with spikes truncated. Solid circles are mixed PSPs. Open circles are in gabazine. ***$p < 0.001$; n.s. = not significant ($p > 0.05$), Tukey's multiple comparisons tests. *N* = (cells/mice). ***H***, Number of action potentials resulting from theta burst stimulation in ACSF and GBZ. ***$p < 0.001$; n.s. = not significant ($p > 0.05$), Sidak's multiple comparisons tests. ***I***, Example traces of postsynaptic currents in response to theta-burst stimulation of Schaffer collaterals at the mid stim intensity (3× threshold) in WT (left) and KO (right) when QX-314 (5 mM) was included in the intracellular solution to block active membrane properties. ***J***, No difference in PSPs, measured as area under the curve, for a range of stimulation intensities between WT and KO neurons with intracellular QX-314 [n.s. = not significant ($p > 0.05$), main effect of genotype, RM ANOVA].

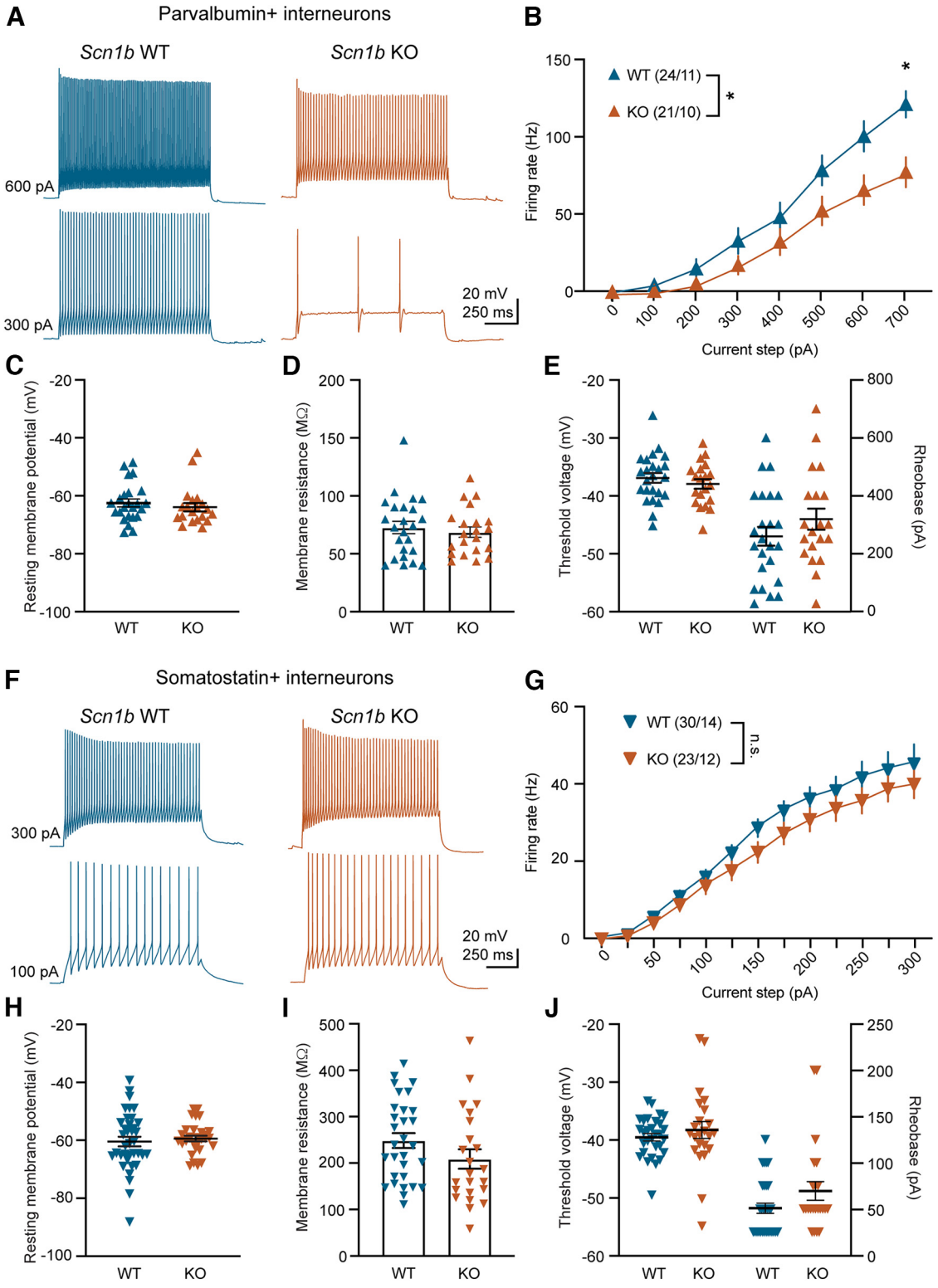

Figure 7. Reduced firing in PV+ but not SST+ interneurons from *Scn1b* KO mice. ***A***, Example traces from WT (left, blue) and KO (right, orange) parvalbumin (PV) expressing interneurons in response to current injections of 300 pA (bottom) and 600 pA (top). ***B***, F/I plot from PV+ interneurons showing that KO neurons fire less than WT neurons. $*p < 0.05$, main effect of genotype, two-way RM ANOVA, $*p = 0.012$ between genotype comparison at 700 pA, Sidak's multiple comparison's test. N = cells/mice. ***C***, There was no difference in resting membrane potential, (***D***) membrane resistance, (***E***) voltage threshold (left), or rheobase (right) between genotypes in PV+ neurons**.** ***F***, Example traces of from WT (left, blue) and KO (right, orange) somatostatin (SST)-expressing interneurons in response to current injections of 100 pA (bottom) and 300 pA (top). ***G***, F/I plot from SST+ interneurons. n.s. $= p > 0.05$, main effect of genotype, two-way RM ANOVA. ***H***, KO SST+ interneurons showed no difference in (***H***) resting membrane potential, (***I***) membrane resistance, (***J***) voltage threshold (left), or rheobase (right) between genotypes.

Table 5. Interneuron physiology

Figure	Experiment	ANOVA main effects
7*B*	PV firing	Current injection: $F_{(2.168,90.74)} = 112.0$, $p < 0.0001$ Genotype: $F_{(1,43)} = 6.384$, $p = 0.015$ Current × genotype: $F_{(7,693)} = 4.852$, $p < 0.0001$
7*G*	SST firing	Current injection: $F_{(1.60,81.55)} = 98.39$, $p < 0.0001$ Genotype: $F_{(1,51)} = 1.968$, $p = 0.167$ Current × genotype: $F_{(12,612)} = 0.495$, $p = 0.918$
8*B*, left	PV theta firing 1× stim	Theta cycle $F_{(4,110)} = 0.273$, $p = 0.89$ Genotype: $F_{(1,110)} = 2.001$, $p = 0.160$ Theta cycle × genotype: $F_{(4,110)} = 0.192$, $p = 0.942$
8*B*, middle	PV theta firing 3× stim	Theta cycle $F_{(4,110)} = 0.076$, $p = 0.989$ Genotype: $F_{(1,110)} = 4.682$, $p = 0.033$ Theta cycle × genotype: $F_{(4,110)} = 0.033$, $p = 0.998$
8*B*, right	PV theta firing 5× stim	Theta cycle $F_{(4,110)} = 0.889$, $p = 0.473$ Genotype: $F_{(1,110)} = 16.18$, $p = 0.0001$ Theta cycle × genotype: $F_{(4,110)} = 0.255$, $p = 0.906$
8*D*, left	SST theta firing 1× stim	Theta cycle: $F_{(1.1,18.7)} = 0.961$, $p = 0.348$ Genotype: $F_{(1,17)} = 7.318$, $p = 0.015$ Theta cycle × genotype: $F_{(4,68)} = 1.170$, $p = 0.332$
8*D*, middle	SST theta firing 3× stim	Theta cycle: $F_{(1.6,26.7)} = 2.835$, $p = 0.087$ Genotype: $F_{(1,17)} = 15.20$, $p = 0.001$ Theta cycle × genotype: $F_{(4,68)} = 4.794$, $p = 0.002$
8*D*, right	SST theta firing 5× stim	Theta cycle: $F_{(1.8,30.4)} = 1.601$, $p = 0.219$ Genotype: $F_{(1,17)} = 13.37$, $p = 0.002$ Theta cycle × genotype: $F_{(4,68)} = 2.938$, $p = 0.027$

All comparisons are two-way repeated measures ANOVAs.

interactions with α subunits of voltage-gated sodium channels (Hartshorne and Catterall, 1984; Messner et al., 1986; Isom et al., 1992), $\beta 1$ also interacts with and modulates potassium channels involved in action potential repolarization and dendritic integration (Deschênes and Tomaselli, 2002; Marionneau et al., 2012; Nguyen et al., 2012). The extracellular domain of $\beta 1$ serves as a cell adhesion molecule (Davis et al., 2004; Brackenbury et al., 2010; Patino et al., 2011), and the intracellular domain regulates neurite outgrowth (Brackenbury et al., 2008) or can be cleaved and translocate to the nucleus to alter transcription (Bouza et al., 2021). The diverse functions of *SCN1B* indicate multiple pathways through which its loss could disrupt neurophysiology, complicating the question of whether phenotypes are primary to loss of protein function, compensatory mechanisms, or driven by seizures that wrack the circuitry. For example, reduced action potential amplitude in pyramidal neurons and decreased firing in PV+ interneurons are consistent with a role for $\beta 1$ in stabilizing surface expression of and increasing conductance through sodium channels, thus likely a direct result of *Scn1b* loss.

A surprising finding is increased sag voltage in *Scn1b* KO pyramidal neurons. There is no known direct interaction between $\beta 1$ and HCN channels, which mediate I_h and voltage sag. HCN channels in pyramidal neurons have a gradient of increasing expression from soma to distal dendrites where they suppress synaptic integration and activity (Magee, 1998; Lörincz et al., 2002). The mechanism for increased somatic HCN channels activity described here is not clear, but functionally it decreases input resistance in opposition to lower capacitance of smaller somata. More somatic HCN channels may be because of disrupted dendritic trafficking, which would amplify synaptic inputs (Magee, 1999; Shin et al., 2008), consistent with the enhanced synaptic integration revealed here. We found that HCN channel gene expression is not upregulated, which can occur as a homeostatic response to counteract enhanced excitability (van Welie et al., 2004; Fan et al., 2005). Alternately, it may be a developmental delay in channel regulation, as somatic HCN channel density is higher in immature neurons to counteract high input resistance (Yang et al., 2013). Interestingly, voltage sag upregulation was recently reported in the *Scn1a* mouse model of Dravet syndrome (Jones et al., 2022), and HCN gain of function variants have been linked to severe early infantile epileptic encephalopathy (Nava et al., 2014), suggesting this may be a widespread neurophysiological change associated with DEEs. Both gain-of-function and loss-of-function HCN variants have been linked to a range of epilepsy disorders (Marini et al., 2018; Kessi et al., 2022), and alterations in HCN channel function has been reported in response to epilepsy and seizures (K. Chen et al., 2001; Jung et al., 2007, 2011; Brennan et al., 2016). Thus, investigating HCN channels multifaceted roles in modulating neuronal physiology may be important across genetic DEE models.

Prior studies on *Scn1b* loss document mixed physiological changes varying by cell type, brain area, preparation, and model. Reid et al. (2014) found increased excitability in Layer (L) 2/3 cortical and subicular pyramidal neurons, while CA1 and L5 cortical pyramidal neurons exhibited unchanged physiology in a *Scn1b* LOF pathologic variant model. Hull et al. (2020) show that *Scn1b* KO L6 and subicular pyramidal neurons displayed increased firing to small current injections but go into depolarization block earlier than WT. They observed no change in L5 pyramidal cell firing, whereas Marionneau et al. (2012) found increased firing. In CA1 pyramidal neurons, we found a modest increase in firing in response to larger amplitude current steps, without a change in resting membrane potential, voltage threshold, or rheobase. These data collectively indicate that subtle increases in intrinsic somatic excitability of pyramidal neurons likely contribute to the epileptic phenotype of *Scn1b* loss but is not the only source of dysfunction.

Another level of neuronal processing altered in *Scn1b* null hippocampus is synaptic transmission. Our data demonstrate a surprising reduction in postsynaptic excitatory and inhibitory current amplitudes, without changing excitatory/inhibitory ratio. The smaller currents are substantially more facilitating in KOs compared with WT, likely contributing to enhanced integration of inputs and indicating changes to neurotransmitter release. Increased paired-pulse ratio in field potential recordings has been reported at various locations including CA1, CA3, dentate gyrus, and cortical L2/3 (Brackenbury et al., 2013), indicating that altered release probability and short-term plasticity may be a widespread mechanism of dysfunction in the *Scn1b* null brain. These synaptic alterations combined with relatively subtle increases in somatic excitability would not be expected to produce the greatly enhanced excitability of KO pyramidal neurons in response synaptic stimulations. We hypothesize that dendritic physiology and processing of incoming synaptic inputs is altered in *Scn1b* KO pyramidal cells. The physiological properties of dendrites are unique and independent from the cell body, as dendritic morphology and distribution of ion channels act to dampen or enhance signal propagation (Spruston, 2008). We did not find differences in dendritic length or gross dendritic structure, and while we cannot rule out less obvious changes in dendritic morphology, we hypothesize that changes to dendritic ion channels play a role in the enhanced synaptic integration found here. Our QX-314 data supports that active membrane conductances are necessary for the enhanced integration in KO neurons. Furthermore, $\beta 1$ interacts with voltage-gated sodium and potassium channels specifically involved in the control of dendritic excitability (Brackenbury and Isom, 2011; Marionneau et al., 2012; Nguyen et al., 2012), and our data provide evidence of

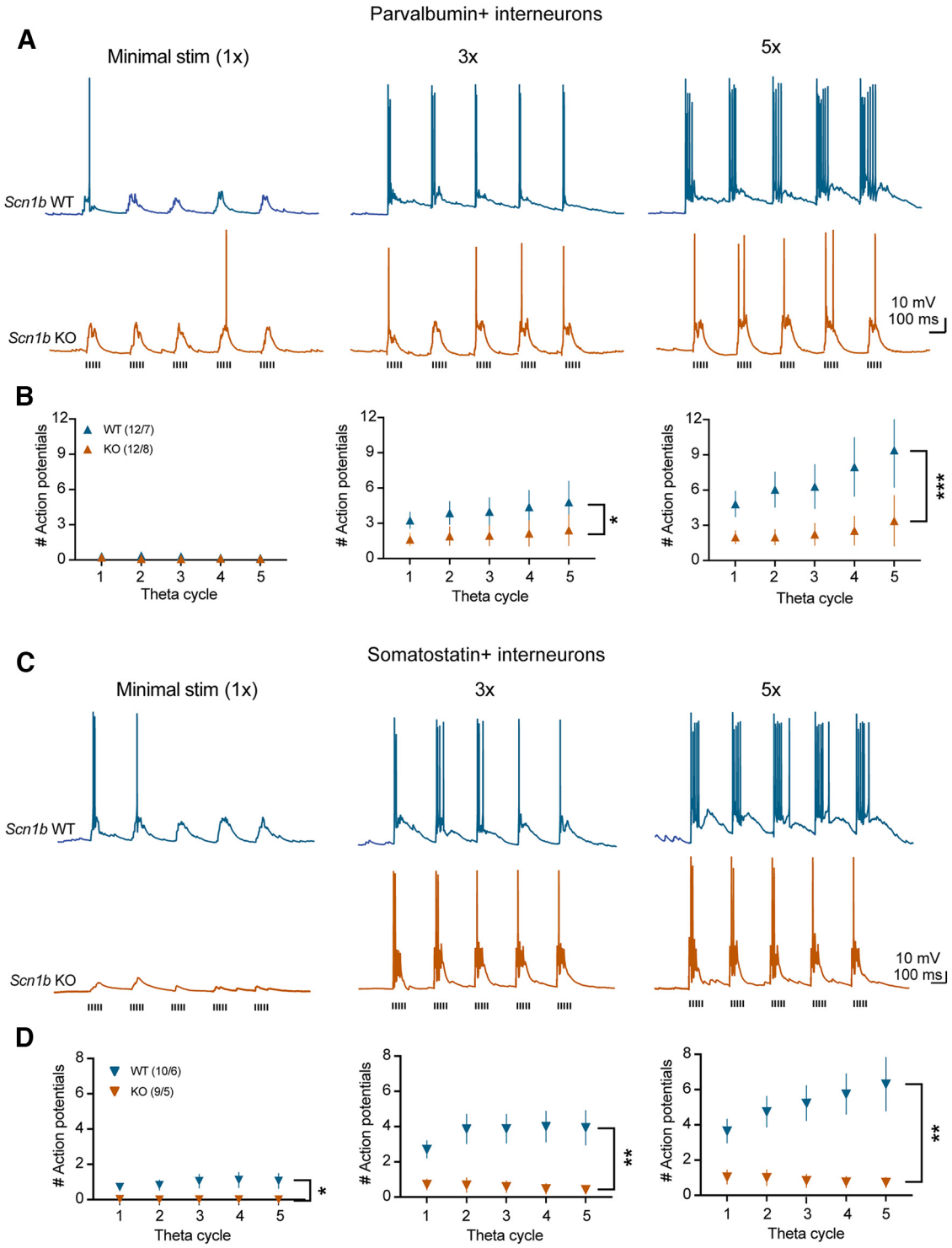

Figure 8. PV+ and SST+ interneurons are less likely to be recruited by theta burst stimulation in the *Scn1b* KO hippocampus. ***A***, Example PSPs recorded from PV+ interneurons from WT (top, blue) or KO (bottom, orange) in response to SC theta burst stimulation at the threshold stimulation intensity (1×; left), 3× (middle), and 5× the threshold intensity (right). ***B***, Number of action potentials per theta cycle at the 1× (left), 3× (middle), and 5× (right) stim intensities. N = cells/mice. *$p < 0.05$, ***$p < 0.001$; main effect of genotype; two-way RM ANOVA. ***C***, Example PSPs recorded from SST+ interneurons from WT (top, blue) or KO (bottom, orange) slices in response to SC theta burst stimulation at 1× (left), 3× (middle), and 5× (right) the threshold intensity. ***D***, Number of action potentials per theta cycle at the 1× (left), 3× (middle), and 5× (right) stim intensities. N = cells/mice. *$p < 0.05$, **$p < 0.01$; main effect of genotype, two-way RM ANOVA.

altered physiology of another primary controller of dendritic excitability: HCN channels (Magee, 1998, 1999). While we were not able to directly measure dendritic physiology here, our data reveal qualitative hints of dendritic hyperexcitability: KO neurons exhibit prolonged depolarization (plateaus) and complex spikes in response to high intensity stimulation or when inhibition is blocked (Figs. 1*A*, 6*F*), suggesting enhanced nonlinear dendritic responses (Spruston, 2008).

Changes to inhibitory interneuron function and excitatory/inhibitory interactions are complex in this and other Dravet

syndrome models (Catterall, 2018; Favero et al., 2018; Almog et al., 2021; Chancey and Howard, 2022; Jones et al., 2022; Mattis et al., 2022). Hull et al. (2020) found that deletion of *Scn1b* isolated to PV+ interneurons was sufficient to cause reductions in excitability and sodium currents in cortical PV+ neurons, seizures, and 100% mortality in mice by P35 (compared with P22 for constitutive *Scn1b* null mice). On the other hand, Reid et al. (2014) found no change to hippocampal fast-spiking (putative PV+) interneuron excitability in a constitutive mouse model homozygous for a human null Scn1b variant. Here, we show that hippocampal PV+ fast-spiking interneurons from KOs had decreased firing in response to current injections, while firing properties in SST+ stratum oriens interneurons were normal, indicating that loss of *Scn1b* has cell specific effects. We measured interneuron recruitment by physiologically relevant theta-patterned synaptic stimulation, and found activation of both interneuron subtypes is greatly diminished in *Scn1b* null slices. Despite changes to interneuron physiology, blockade of $GABA_A$ receptors caused a massive increase in activity in KO pyramidal neurons compared with WT in response to synaptic stimulation. Thus, synaptic inhibition is clearly exerting a great deal of control over excitability of pyramidal neurons in the KO brain during ongoing activity. Finally, Yuan et al. (2019) found that the developmental shift in chloride reversal potential is delayed in *Scn1b* KOs. This is mitigated in our experiments by whole cell recording, but could greatly complicate excitatory/inhibitory interactions *in vivo*. Overall, changes to interneuron subtypes' physiology and their inhibitory control of other neurons, are deeply complex and likely alter information processing by hippocampal circuitry.

DEEs are complex disorders with a diverse array of cognitive delays and dysfunction and are often resistant to treatment with antiseizure medications. Neuronal information processing underlying these cognitive functions relies on interplay between synaptic properties, dendritic intrinsic properties that amplify or suppress synaptic signals to integrate them over space and time, and firing properties that produce neuronal output. We have shown that loss of *Scn1b* results in complex neuronal dysfunction all levels of neuronal information processing: synaptic inputs; inhibitory drive; synaptic integration; somatic intrinsic physiology; and action potential firing. We hypothesize that the nuanced physiological changes and fundamental change in cellular information processing in the hippocampus revealed here may underlie the complexity of the seizures and associated cognitive defects in *SCN1B*-linked epileptic encephalopathies and the ineffectiveness of drugs that target a single aspect of neuronal physiology.

References

Aeby A, Sculier C, Bouza AA, Askar B, Lederer D, Schoonjans AS, Vander Ghinst M, Ceulemans B, Offord J, Lopez-Santiago LF, Isom LL (2019) SCN1B-linked early infantile developmental and epileptic encephalopathy. Ann Clin Transl Neurol 6:2354–2367.

Albertson AJ, Bohannon AS, Hablitz JJ (2017) HCN channel modulation of synaptic integration in GABAergic interneurons in malformed rat neocortex. Front Cell Neurosci 11:109.

Almog Y, Fadila S, Brusel M, Mavashov A, Anderson K, Rubinstein M (2021) Developmental alterations in firing properties of hippocampal CA1 inhibitory and excitatory neurons in a mouse model of Dravet syndrome. Neurobiol Dis 148:105209.

Arnold EC, McMurray C, Gray R, Johnston D (2019) Epilepsy-induced reduction in HCN channel expression contributes to an increased excitability in dorsal, but not ventral, hippocampal CA1 neurons. eNeuro 6:ENEURO.0036-19.2019.

Bouza AA, Edokobi N, Hodges SL, Pinsky AM, Offord J, Piao L, Zhao YT, Lopatin AN, Lopez-Santiago LF, Isom LL (2021) Sodium channel β1 subunits participate in regulated intramembrane proteolysis-excitation coupling. JCI Insight 6:e141776.

Brackenbury WJ, Isom LL (2011) Na channel β subunits: overachievers of the ion channel family. Front Pharmacol 2:53.

Brackenbury WJ, Davis TH, Chen C, Slat EA, Detrow MJ, Dickendesher TL, Ranscht B, Isom LL (2008) Voltage-gated Na+ channel beta1 subunit-mediated neurite outgrowth requires Fyn kinase and contributes to post-natal CNS development in vivo. J Neurosci 28:3246–3256.

Brackenbury WJ, Calhoun JD, Chen C, Miyazaki H, Nukina N, Oyama F, Ranscht B, Isom LL (2010) Functional reciprocity between Na+ channel Nav1.6 and beta1 subunits in the coordinated regulation of excitability and neurite outgrowth. Proc Natl Acad Sci U S A 107:2283–2288.

Brackenbury WJ, Yuan Y, O'Malley HA, Parent JM, Isom LL (2013) Abnormal neuronal patterning occurs during early postnatal brain development of Scn1b-null mice and precedes hyperexcitability. Proc Natl Acad Sci U S A 110:1089–1094.

Brennan GP, Baram TZ, Poolos NP (2016) Hyperpolarization-activated cyclic nucleotide-gated (HCN) channels in epilepsy. Cold Spring Harb Perspect Med 6:a022384.

Catterall WA (2018) Dravet syndrome: a sodium channel interneuronopathy. Curr Opin Physiol 2:42–50.

Chancey JH, Howard MA (2022) Synaptic integration in CA1 pyramidal neurons is intact despite deficits in GABAergic transmission in the *Scn1a* haploinsufficiency mouse model of Dravet syndrome. eNeuro 9: ENEURO.0080-22.2022.

Chen C, Westenbroek RE, Xu X, Edwards CA, Sorenson DR, Chen Y, McEwen DP, O'Malley HA, Bharucha V, Meadows LS, Knudsen GA, Vilaythong A, Noebels JL, Saunders TL, Scheuer T, Shrager P, Catterall WA, Isom LL (2004) Mice lacking sodium channel beta1 subunits display defects in neuronal excitability, sodium channel expression, and nodal architecture. J Neurosci 24:4030–4042.

Chen K, Aradi I, Thon N, Eghbal-Ahmadi M, Baram TZ, Soltesz I (2001) Persistently modified h-channels after complex febrile seizures convert the seizure-induced enhancement of inhibition to hyperexcitability. Nat Med 7:331–337.

Davis TH, Chen C, Isom LL (2004) Sodium channel beta1 subunits promote neurite outgrowth in cerebellar granule neurons. J Biol Chem 279:51424–51432.

Deschênes I, Tomaselli GF (2002) Modulation of Kv4.3 current by accessory subunits. FEBS Lett 528:183–188.

Dougherty KA, Nicholson DA, Diaz L, Buss EW, Neuman KM, Chetkovich DM, Johnston D (2013) Differential expression of HCN subunits alters voltage-dependent gating of h-channels in CA1 pyramidal neurons from dorsal and ventral hippocampus. J Neurophysiol 109:1940–1953.

Fan Y, Fricker D, Brager DH, Chen X, Lu HC, Chitwood RA, Johnston D (2005) Activity-dependent decrease of excitability in rat hippocampal neurons through increases in I(h). Nat Neurosci 8:1542–1551.

Favero M, Sotuyo NP, Lopez E, Kearney JA, Goldberg EM (2018) A transient developmental window of fast-spiking interneuron dysfunction in a mouse model of Dravet syndrome. J Neurosci 38:7912–7927.

Hartshorne RP, Catterall WA (1984) The sodium channel from rat brain. Purification and subunit composition. J Biol Chem 259:1667–1675.

Haworth AS, Hodges SL, Capatina AL, Isom LL, Baumann CG, Brackenbury WJ (2022) Subcellular dynamics and functional activity of the cleaved intracellular domain of the Na. J Biol Chem 298:102174.

Honsa P, Pivonkova H, Harantova L, Butenko O, Kriska J, Dzamba D, Rusnakova V, Valihrach L, Kubista M, Anderova M (2014) Increased expression of hyperpolarization-activated cyclic nucleotide-gated (HCN) channels in reactive astrocytes following ischemia. Glia 62:2004–2021.

Howard MA, Baraban SC (2017) Catastrophic epilepsies of childhood. Annu Rev Neurosci 40:149–166.

Hull JM, Isom LL (2018) Voltage-gated sodium channel β subunits: the power outside the pore in brain development and disease. Neuropharmacology 132:43–57.

Hull JM, O'Malley HA, Chen C, Yuan Y, Denomme N, Bouza AA, Anumonwo C, Lopez-Santiago LF, Isom LL (2020) Excitatory and inhibitory neuron defects in a mouse model of Scn1b-linked EIEE52. Ann Clin Transl Neurol 7:2137–2149.

Isaac JT, Wheal HV (1993) The local anaesthetic QX-314 enables enhanced whole-cell recordings of excitatory synaptic currents in rat hippocampal slices in vitro. Neurosci Lett 150:227–230.

Isom LL, De Jongh KS, Patton DE, Reber BF, Offord J, Charbonneau H, Walsh K, Goldin AL, Catterall WA (1992) Primary structure and functional expression of the beta 1 subunit of the rat brain sodium channel. Science 256:839–842.

Jones SP, O'Neill N, Muggeo S, Colasante G, Kullmann DM, Lignani G (2022) Developmental instability of CA1 pyramidal cells in Dravet syndrome. bioRxiv 507264. https://doi.org/10.1101/2022.09.12.507264.

Jung S, Jones TD, Lugo JN, Sheerin AH, Miller JW, D'Ambrosio R, Anderson AE, Poolos NP (2007) Progressive dendritic HCN channelopathy during epileptogenesis in the rat pilocarpine model of epilepsy. J Neurosci 27:13012–13021.

Jung S, Warner LN, Pitsch J, Becker AJ, Poolos NP (2011) Rapid loss of dendritic HCN channel expression in hippocampal pyramidal neurons following status epilepticus. J Neurosci 31:14291–14295.

Kessi M, Peng J, Duan H, He H, Chen B, Xiong J, Wang Y, Yang L, Wang G, Kiprotich K, Bamgbade OA, He F, Yin F (2022) The contribution of HCN channelopathies in different epileptic syndromes, mechanisms, modulators, and potential treatment targets: a systematic review. Front Mol Neurosci 15:807202.

Kole MH, Stuart GJ (2012) Signal processing in the axon initial segment. Neuron 73:235–247.

Livak KJ, Schmittgen TD (2001) Analysis of relative gene expression data using real-time quantitative PCR and the 2(-Delta Delta C(T)) method. Methods 25:402–408.

Lopez-Santiago LF, Meadows LS, Ernst SJ, Chen C, Malhotra JD, McEwen DP, Speelman A, Noebels JL, Maier SK, Lopatin AN, Isom LL (2007) Sodium channel Scn1b null mice exhibit prolonged QT and RR intervals. J Mol Cell Cardiol 43:636–647.

Lörincz A, Notomi T, Tamás G, Shigemoto R, Nusser Z (2002) Polarized and compartment-dependent distribution of HCN1 in pyramidal cell dendrites. Nat Neurosci 5:1185–1193.

Magee JC (1998) Dendritic hyperpolarization-activated currents modify the integrative properties of hippocampal CA1 pyramidal neurons. J Neurosci 18:7613–7624.

Magee JC (1999) Dendritic Ih normalizes temporal summation in hippocampal CA1 neurons. Nat Neurosci 2:848.

Marini C, et al. (2018) HCN1 mutation spectrum: from neonatal epileptic encephalopathy to benign generalized epilepsy and beyond. Brain 141:3160–3178.

Marionneau C, Carrasquillo Y, Norris AJ, Townsend RR, Isom LL, Link AJ, Nerbonne JM (2012) The sodium channel accessory subunit Navβ1 regulates neuronal excitability through modulation of repolarizing voltage-gated K^+ channels. J Neurosci 32:5716–5727.

Mattis J, Somarowthu A, Goff KM, Jiang E, Yom J, Sotuyo N, Mcgarry LM, Feng H, Kaneko K, Goldberg EM (2022) Corticohippocampal circuit dysfunction in a mouse model of Dravet syndrome. Elife 11:e69293.

Messner DJ, Feller DJ, Scheuer T, Catterall WA (1986) Functional properties of rat brain sodium channels lacking the beta 1 or beta 2 subunit. J Biol Chem 261:14882–14890.

Moosmang S, Biel M, Hofmann F, Ludwig A (1999) Differential distribution of four hyperpolarization-activated cation channels in mouse brain. Biol Chem 380:975–980.

Müller C, Remy S (2014) Dendritic inhibition mediated by O-LM and bistratified interneurons in the hippocampus. Front Synaptic Neurosci 6:23.

Nava C, et al. (2014) De novo mutations in HCN1 cause early infantile epileptic encephalopathy. Nat Genet 46:640–645.

Nguyen HM, Miyazaki H, Hoshi N, Smith BJ, Nukina N, Goldin AL, Chandy KG (2012) Modulation of voltage-gated K+ channels by the sodium channel β1 subunit. Proc Natl Acad Sci U S A 109:18577–18582.

Oda M, Yoshida A, Ikemoto Y (1992) Blockade by local anaesthetics of the single Ca(2+)-activated K+ channel in rat hippocampal neurones. Br J Pharmacol 105:63–70.

Ogiwara I, Nakayama T, Yamagata T, Ohtani H, Mazaki E, Tsuchiya S, Inoue Y, Yamakawa K (2012) A homozygous mutation of voltage-gated sodium channel β(I) gene SCN1B in a patient with Dravet syndrome. Epilepsia 53:e200–e203.

O'Malley HA, Hull JM, Clawson BC, Chen C, Owens-Fiestan G, Jameson MB, Aton SJ, Parent JM, Isom LL (2019) deletion in adult mice results in seizures and SUDEP. Ann Clin Transl Neurol 6:1121–1126.

Patino GA, Claes LR, Lopez-Santiago LF, Slat EA, Dondeti RS, Chen C, O'Malley HA, Gray CB, Miyazaki H, Nukina N, Oyama F, De Jonghe P, Isom LL (2009) A functional null mutation of SCN1B in a patient with Dravet syndrome. J Neurosci 29:10764–10778.

Patino GA, Brackenbury WJ, Bao Y, Lopez-Santiago LF, O'Malley HA, Chen C, Calhoun JD, Lafrenière RG, Cossette P, Rouleau GA, Isom LL (2011) Voltage-gated Na+ channel β1B: a secreted cell adhesion molecule involved in human epilepsy. J Neurosci 31:14577–14591.

Pelkey KA, Chittajallu R, Craig MT, Tricoire L, Wester JC, McBain CJ (2017) Hippocampal GABAergic inhibitory interneurons. Physiol Rev 97:1619–1747.

Perkins KL, Wong RK (1995) Intracellular QX-314 blocks the hyperpolarization-activated inward current Iq in hippocampal CA1 pyramidal cells. J Neurophysiol 73:911–915.

Poolos NP, Migliore M, Johnston D (2002) Pharmacological upregulation of h-channels reduces the excitability of pyramidal neuron dendrites. Nat Neurosci 5:767–774.

Reid CA, Leaw B, Richards KL, Richardson R, Wimmer V, Yu C, Hill-Yardin EL, Lerche H, Scheffer IE, Berkovic SF, Petrou S (2014) Reduced dendritic arborization and hyperexcitability of pyramidal neurons in a Scn1b-based model of Dravet syndrome. Brain 137:1701–1715.

Scheffer IE, Harkin LA, Grinton BE, Dibbens LM, Turner SJ, Zielinski MA, Xu R, Jackson G, Adams J, Connellan M, Petrou S, Wellard RM, Briellmann RS, Wallace RH, Mulley JC, Berkovic SF (2007) Temporal lobe epilepsy and GEFS+ phenotypes associated with SCN1B mutations. Brain 130:100–109.

Shin M, Brager D, Jaramillo TC, Johnston D, Chetkovich DM (2008) Mislocalization of h channel subunits underlies h channelopathy in temporal lobe epilepsy. Neurobiol Dis 32:26–36.

Spruston N (2008) Pyramidal neurons: dendritic structure and synaptic integration. Nat Rev Neurosci 9:206–221.

Strauss U, Kole MH, Bräuer AU, Pahnke J, Bajorat R, Rolfs A, Nitsch R, Deisz RA (2004) An impaired neocortical Ih is associated with enhanced excitability and absence epilepsy. Eur J Neurosci 19:3048–3058.

Stuart GJ, Spruston N (2015) Dendritic integration: 60 years of progress. Nat Neurosci 18:1713–1721.

Surges R, Brewster AL, Bender RA, Beck H, Feuerstein TJ, Baram TZ (2006) Regulated expression of HCN channels and cAMP levels shape the properties of the h current in developing rat hippocampus. Eur J Neurosci 24:94–104.

Talbot MJ, Sayer RJ (1996) Intracellular QX-314 inhibits calcium currents in hippocampal CA1 pyramidal neurons. J Neurophysiol 76:2120–2124.

van Welie I, van Hooft JA, Wadman WJ (2004) Homeostatic scaling of neuronal excitability by synaptic modulation of somatic hyperpolarization-activated Ih channels. Proc Natl Acad Sci U S A 101:5123–5128.

Yang YS, Kang MS, Kim SH, Kim SJ, Eun SY, Kwon OB, Jung SC (2013) I(h) channels prevent overexcitability of early developmental CA1 neurons showing high input resistance in rats. Brain Res Bull 91:14–20.

Yuan Y, O'Malley HA, Smaldino MA, Bouza AA, Hull JM, Isom LL (2019) Delayed maturation of GABAergic signaling in the Scn1a and Scn1b mouse models of Dravet syndrome. Sci Rep 9:6210.